

1 2700 years of Mediterranean environmental change in central Italy: A synthesis of sedimentary and
2 cultural records to interpret past impacts of climate on society

3

4 Scott A. Mensing^{1*}, Irene Tunno², Leonardo Sagnotti³, Fabio Florindo³, Paula Noble⁴, Claire Archer⁴,
5 Susan Zimmerman⁵, Francisco-Javier Pavón-Carrasco³, Gabriele Cifani⁶, Susanna Passigli⁶, Gianluca
6 Piovesan²

7

8 ¹Department of Geography, University of Nevada, Reno, Nevada, USA

9 ²Dendrology Lab, DAFNE Università degli Studi della Tuscia, Viterbo, Italy

10 ³Istituto Nazionale di Geofisica e Vulcanologia, Rome, Italy

11 ⁴Department of Geosciences, University of Nevada, Reno, Nevada, USA

12 ⁵Center for Accelerator Mass Spectrometry, Lawrence Livermore National Laboratory, California,
13 USA

14 ⁶Università degli Studi di Roma Tor Vergata, Rome, Italy

15

16

17 *Corresponding author smensing@unr.edu

18

19 Running head: 2700 years of Mediterranean environmental change

20

21 Abstract:

22 Abrupt climate change in the past is thought to have disrupted societies by accelerating
23 environmental degradation, potentially leading to cultural collapse. Linking climate change directly
24 to societal disruption is challenging because socioeconomic factors also play a large role, with
25 climate being secondary or sometimes inconsequential. Combining paleolimnologic, historical, and
26 archaeological methods provides for a more secure basis for interpreting the past impacts of climate
27 on society. We present pollen, non-pollen palynomorph, geochemical, paleomagnetic and
28 sedimentary data from a high-resolution 2700 yr lake sediment core from central Italy and compare
29 these data with local historical documents and archeological surveys to reconstruct a record of
30 environmental change in relation to socioeconomic history and climatic fluctuations. Here we
31 document cases in which environmental change is strongly linked to changes in local land
32 management practices in the absence of clear climatic change, as well as examples when climate
33 change appears to have been a strong catalyst that resulted in significant environmental change that
34 impacted local communities. During the Imperial Roman period, despite a long period of stable, mild
35 climate, and a large urban population in nearby Rome, our site shows only limited evidence for
36 environmental degradation. Warm and mild climate during the Medieval Warm period on the other
37 hand led to widespread deforestation and erosion. The ability of the Romans to utilize imported
38 resources through an extensive trade network may have allowed for preservation of the
39 environment near the Roman capital, whereas during Medieval time, the need to rely on local
40 resources led to environmental degradation. Cool wet climate during the Little Ice Age led to a
41 breakdown in local land use practices, widespread land abandonment and rapid reforestation. Our
42 results present a high-resolution regional case study that explores the effect of climate change on
43 society for an under-documented region of Europe.

44

45

46 **1. Introduction**

47 The extent to which past abrupt climate change has directly resulted in societal disruption or cultural
48 collapse, and the ability of societies to adapt to these changes is strongly debated (Berglund, 2003;
49 Diamond, 2005; Munoz et al., 2010), but is potentially significant for modern communities facing
50 future climate change (Büntgen et al., 2011). Studies concerned with the link between climate and
51 human affairs have increasingly recognized the need to examine societal change in parallel with
52 climate change (Dearing et al., 2008; Coombes et al., 2009; Munoz et al., 2010, McCormick et al.,
53 2012), although the tendency persists among physical scientists to link cultural shifts directly to
54 climate change (O’Sullivan, 2008; Aimers, 2011). Detailed historical analyses based on precisely
55 dated documents have identified instances when climate has led to significant societal disruption or
56 ‘collapse’, but these analyses also detail multiple examples in which socioeconomic factors played
57 the larger role in environmental change, with climate being secondary or inconsequential (Ladurie,
58 1971). For this reason, it is critical that studies attempting to elucidate the impact of climate on
59 society closely couple paleoecologic methods with historical and archaeological methods (Dearing et
60 al., 2008; O’Sullivan, 2008; Coombes et al., 2009; Harris, 2013).

61
62 The relationship between climate change and cultural response can be addressed in areas where
63 multi-proxy studies of cores from lakes with very high sediment accumulation rates can be examined
64 within the context of a well-documented written history (Berglund, 2003). Such a history may
65 provide insights into human adaptive strategies that allowed societies to cope with past climate
66 change (Fraser, 2010). Several recent high-resolution syntheses have drawn a link between climate
67 stability and the expansion, and eventual contraction of the Roman Empire (Büntgen et al., 2011;
68 McCormick et al., 2012). These studies note that focused regional case studies with highly resolved
69 datasets are still needed to test the potential effect of rapid climate change on human societies.
70 Such datasets are particularly needed in under-documented regions of the Roman Empire, including
71 southern Europe, and the regions near Rome.

72

73 In central Italy, archival materials are nearly continuously available from ~700 CE (common era) in
74 the records of the Farfa Abbey (Leggio, 1995a) in northern Lazio, Central Italy, with some written
75 records extending back to the Roman period (De Santis and Coarelli, 2009). These documents
76 provide a written environmental history that can be compared with physical paleoecologic
77 reconstructions. Paleoecologic reconstructions for the last 3000 years are still underrepresented in
78 Italy (Roberts et al., 2004; Magri, 2007) with studies from the southern Alps and North Italy (Joannin
79 et al., 2014; Kaltenrieder et al. 2010), the northern and central Apennines (e.g. Mercuri et al., 2002;
80 Branch and Marini, 2013; Brown et al., 2013), the Tiber Delta (Di Rita et al., 2010), and southern
81 Italy, Sicily and Sardinia (e.g. Russo Ermolli and Di Pasquale, 2002; Di Rita and Magri, 2009; Tinner et
82 al., 2009; Di Rita and Mellis, 2013; Sadori et al., 2013). These studies record the major changes in
83 vegetation in relation to human activity during this time period but present very different impacts
84 depending on sites and historical periods. In addition, the sampling resolution is generally at the
85 centennial or millennial scale and cannot be easily compared with historical records. The last 3000
86 years are of particular interest because they encompass several important climatic changes often
87 associated with cultural change, including the Roman Optimum (100 BCE – 200 CE; BCE – before
88 common era), the Medieval Warm Period (MWP), ~950 to 1250 CE, and the Little Ice Age (LIA)
89 ~1250 to 1850 CE, (Büntgen et al., 2011; Christiansen and Ljungqvist, 2012; McCormick et al., 2012).

90

91 In this paper, we present multiple physical proxies (pollen, non-pollen palynomorphs,
92 paleomagnetism, sedimentology, geochemistry and charcoal) from a small lake in the Rieti Basin,
93 Central Italy, to reconstruct a high-resolution record of environmental history from the present
94 through the pre-Roman period. The basin, located approximately 80 km north of Rome, has a well-
95 documented archeological record from pre-Roman times (Coccia et al., 1992) and historical
96 documents from early Roman times (Coccia et al., 1992; Leggio, 1995a). We compare our physical
97 proxies with the well-documented historical record of human activity and cultural change, and with

98 independent climate records to explore the link between the timing of climate change,
99 environmental change, and historical events. This study complements previous high-resolution
100 regional syntheses from central and northern Europe (Ladurie, 1971; Büntgen et al., 2011;
101 McCormick et al., 2012) by providing a new site in southern Europe at the center of the Roman
102 Empire. The results contribute to our understanding of Mediterranean forest dynamics and can be
103 used to verify recent efforts to model the history of deforestation in Europe (Kaplan et al., 2009).

104

105 **2. Study Area**

106 Lago Lungo (369 m above mean sea level) is one of four remnant lakes of ancient *Lacus Velinus* in
107 the Rieti Basin (Fig. 1), an intermontane depression in the Central Apennines that locally reach an
108 elevation of 2217 m at Monti Reatini (Calderoni et al., 1994). The Velino, Salto and Turano Rivers
109 flow into the basin, which is then drained by the Velino River, which plummets over a travertine sill
110 at Marmore Falls. Other sources of inflow into the basin are numerous artesian springs that lie along
111 the eastern edge of the basin. Water level in the basin is controlled by the elevation of the travertine
112 sill (Calderoni et al., 1994). During prehistoric time, travertine built up during warm periods, raising
113 the sill and expanding wetlands, and alternatively eroded during cold periods draining the valley
114 (Calderini et al., 1998; Soligo et al., 2002). Between ~6000 and 3000 yr BP a large shallow lake (*Lacus*
115 *Velinus*) filled the basin (Calderoni et al., 1994). Written documents suggest that the Romans cut a
116 channel through the travertine sill to drain the land in ~270 BCE (Coccia et al., 1992). Since that time,
117 water level in the basin has been controlled periodically by maintaining existing channels and cutting
118 new channels (Lorenzetti, 1989). Historical maps suggest that the size and shape of lakes, their
119 proximity to the Velino River, and the extent of wetlands in the basin has changed through time.
120 Today, Lago Lungo has a maximum depth of up to 7 m with a surface area of 0.78 km² and surface
121 level maintained at 369 m above sea level (Riccardi, 2006). Inflow is from a network of ditches that
122 drain surrounding wetlands, springs, and farmland. Lago Lungo is protected within Riserva Naturale
123 dei Laghi Lungo e Ripasottile (Riccardi, 2006).

124

125 The geology of the region is characterized by recently uplifted marine sediments. The Central
126 Apennines are primarily composed of Upper Triassic to Middle Miocene carbonates (Parotto and
127 Praturlon, 1975; Coesentino et al., 2010). Rieti is a seismically active extensional basin within the
128 Apennine thrust system and is partially filled with Upper Pliocene and Holocene continental and
129 marine sediments (Cavinato and De Celles, 1999; Soligo et al., 2002). Travertine outcrops are present
130 across the basin, associated with past periods of warm wet climate. Seismic activity has influenced
131 the location and discharge of springs responsible for depositing the travertines (Soligo et al., 2002).
132 The largest spring in the basin, Santa Susanna Spring, has a discharge of $4.1 \text{ m}^3 \text{ s}^{-1}$ and is located ~3
133 km northeast of Lago Lungo (Spadoni et al., 2010)

134

135 Modern vegetation is dominated by agriculture in the basin and heavily managed forest on the
136 surrounding slopes. *Phragmites* and *Salix* species grow in a narrow (~15 m) band of protected land
137 within the reserve, while beyond the reserve border the basin floor is nearly entirely devoted to
138 agriculture (Casella et al., 2009). Forest vegetation at lower elevations within the basin is
139 characterized by temperate deciduous forest (e.g. *Carpinus betulus* L., *Fraxinus* spp., *Ulmus*
140 *campestris* Auct.) with an important submediterranean component (*Quercus pubescens* Willd. and
141 *Q. cerris* L.; *Carpinus orientalis* Miller; *Ostrya carpinifolia* Scop.); in the foothills on steep/shallow
142 soils some patches of Mediterranean trees and shrubs (*Quercus ilex* L., *Phyllirea variabilis* L., *Pinus*
143 *halepensis* Miller) are present while in the mountain belt (above 800-900 m) beech (*Fagus sylvatica*
144 L.) forests are common. Climatically the area is within a transition zone between warm and cool
145 temperate climates with a Mediterranean precipitation pattern characterized by low precipitation
146 during summer. Mean annual temperature varies between 4 °C in January and 21 °C in July with
147 annual precipitation of 1117 mm (Fig. 4.29 in Leone, 2004). The general temperature and
148 precipitation regime is strongly controlled by the North Atlantic Oscillation (NAO) with warm dry

149 climate predominating during positive phases of the NAO, and cool wet climate during negative
150 phases (Hurrell, 1995).

151

152 **3. Materials and Methods**

153 *3.1 Core recovery*

154 Previous studies of Lago Lungo recovered cores on land near the lakeshore using geologic drilling
155 equipment and subsequently did not recover the upper sediments containing the last few thousand
156 years (Calderoni et al., 1994). For this study, we worked on a floating platform anchored near the
157 center of the lake. Cores were collected in 2009 and in 2012. Water depth at the core site was 4.2 m
158 in 2009 and 4.4 m in 2012. Surface sediments were obtained using a clear plastic tube fit with a
159 piston to recover the sediment-water interface (core LUN12-2C). The unconsolidated surface
160 sediments were stabilized with Zorbitrol (sodium polyacrylate absorbent powder) while the core was
161 still in an upright position. Overlapping cores (LUN09 in 2009 and LUN12-1A, 1B, 2A, and 2B in 2012)
162 were recovered with a modified square-rod Livingstone hand operated corer, extruded directly into
163 rigid ABS (Acrylonitrile Butadiene Styrene) plastic tubing, and capped for transport.

164

165 LUN09 spanned sediment depths from 54 to 605 cm and was recovered in six sections. We used GPS
166 to relocate the LUN09 core site in 2012 for taking the next set of cores. Cores LUN12-1A and 1B were
167 taken within 2 m of each other and spanned from 10 to 870 cm depth (ten sections) and 60 to 1028
168 cm depth (twelve sections) respectively. Cores LUN12-2A, 2B and 2C were taken ~10 m from the
169 other set and within 2 m of each other. LUN12-2A spanned from 60 to 1300 cm depth (fifteen
170 sections) and LUN12-2B, the longest core, from 20 to 1438 cm depth (nineteen sections). LUN12-2C,
171 the surface core, contains the sediment-water interface to 123 cm depth.

172

173 LUN-09 was described, analyzed and stored at the Tuscia University Paleoecology Laboratory in
174 Viterbo, Italy. Cores LUN12-1A and 1B were transported to the Tuscia University Paleoecology

175 Laboratory for storage and subsequent u-channel sampling for paleomagnetic analyses. Cores
176 LUN12-2A, 2B- and 1C were shipped to the United States National Lacustrine Core Facility (LacCore)
177 in Minneapolis, Minnesota for initial core description, sampling for pollen, charcoal, smear slide and
178 LOI analysis, and permanent storage.

179

180 *3.2 Initial Core Description and analysis*

181 Core LUN09 was split, photographed and the sediments described in July, 2009. This core was used
182 for pollen analysis of the upper 5 m of core. Cores LUN12-2A, 2B and 2C were first logged whole
183 using a Geotek Multisensor Core Logger to measure density, acoustic wave velocity, electrical
184 resistivity and loop-sensor magnetic susceptibility at 1-cm resolution. Cores were then split, the
185 surface cleaned, imaged with a digital line scanner at ~300 dpi, then placed on a Geotek MSCL-XYZ
186 core scanner and measured at 0.5-cm resolution for magnetic susceptibility and color. Magnetic
187 susceptibility data and core images were input into an electronic standard core description sheet
188 and the sheets annotated for stratigraphy, sedimentology and correlation points between cores
189 using both the images and the freshly split cores. Smear slides, taken every 20 cm and from selected
190 strata, were used to aid in core description and to identify the major sedimentologic components.

191

192 The observed sedimentologic features and magnetic susceptibility data were used to correlate cores
193 LUN12 2A, 2B, and 2C, often allowing for a visual match of individual suites of bands and layers
194 between cores (Figs. 2 and 3). Areas of core distortion, caused by coring artifacts, and sections with
195 no core recovery were identified, and a continuous 'master core,' hereafter referred to as LUN12-2,
196 was constructed from the three cores, that spans a total sedimentary thickness of 14.4 m. Magnetic
197 susceptibility was further used to correlate between core LUN12-2 and LUN12-1A and 1B, and
198 LUN09, which were not photographed nor logged in detail.

199

200 Samples (1.25 cm³) were taken every 10 cm (3-5 cm in sediment transition zones) from LUN12-2 for
201 measuring percent total organic matter (%organic) and percent carbonate (%CaCO₃) using the loss
202 on ignition method protocols at LacCore based on Dean (1974) and Heiri et al. (2001). Samples were
203 weighed, dried at 100 °C for 24 hours, then combusted at 550 °C for four hours followed by
204 combustion at 1000 °C for two hours.

205
206 Core LUN12-2 was transported to the Large Lakes Laboratory in Duluth, Minnesota for analysis using
207 the ITRAX x-ray fluorescence (XRF) scanner (Cox Analytical Instruments) to provide elemental
208 geochemistry data. The LUN12-2 core was scanned at a resolution of 0.5 cm throughout, except for
209 the middle 7 sections (2B-5L through 11L), which were scanned at a resolution of 0.2 cm to pick up
210 observed variations in sedimentary banding. The top section (LUN12-2C) was also scanned at a 0.2
211 cm resolution. The scanner was operated using a molybdenum source, 30 second dwell-time, a
212 voltage of 30 kV and an x-ray current of 30 mA to obtain peak areas for elements Si-Pb. A principal
213 component analysis using the rda function in the vegan 2.0-6 package in R, version 2.1.5.2 (R
214 Development Core Team, 2012) was performed on the raw XRF data output, on both the whole core
215 and on individual sections as an initial data analysis step to determine gross distribution patterns
216 and co-variance of elements. Time series plots for core LUN12-2 were then generated for a subset
217 of elements determined to be of interest as sedimentologic and lake chemistry proxies (Ti, Fe, Mn,
218 Ca, and Sr). Raw counts of the element subset were normalized by centering and standardizing the
219 data (raw data - mean of data / standard deviation), allowing for the comparison of the minima,
220 maxima, and trends of major elements with very different ranges of counts within the core.

221

222 *3.3 Rock magnetism and Paleomagnetism*

223 Natural and artificial magnetizations were measured at room temperature at the paleomagnetic
224 laboratory of the Istituto Nazionale di Geofisica e Vulcanologia (INGV) in Rome, on a narrow-access
225 (45 mm diameter) automated pass through '2G Enterprises' DC 755 superconducting rock

226 magnetometer (SRM), housed in a Lodestar Magnetics shielded room. The cryogenic magnetometer
227 is equipped with in-line orthogonal alternating field (AF) demagnetization coils, with optional
228 application of a single-axis direct current (DC) field for production of an anhysteretic remanent
229 magnetization (ARM). Rock magnetic and paleomagnetic properties were measured at 1-cm spacing
230 on u-channel samples collected from 4 distinct and partly overlapping cores (LUN09, LUN12-1A,
231 LUN12-1B and the lower 5.4 m of LUN12-2B).

232

233 To minimize sample dehydration and alteration, u-channel samples were stored in a refrigerated
234 room until they were processed. For each u-channel, we first measured both the low-field magnetic
235 susceptibility (κ), using a Bartington magnetic susceptibility probe MS2C in-line with the rock
236 magnetometer, and the natural remanent magnetization (NRM). Then, all u-channels were AF
237 demagnetized in 10 steps (using peak fields of 5, 10, 15, 20, 30, 40, 50, 60, 80 and 100 milliTesla
238 (mT), with remanence vectors measured after each demagnetization step, in order to investigate the
239 stability of the NRM and to reveal possible secondary overprints.

240

241 Finally, an ARM was imparted using a 0.05 mT direct current (DC) bias field and an axial 100 mT peak
242 AF, and translating the u-channel through the AF and dc coil system at a speed of 10 cm/s, the
243 lowest speed allowed by the software running the measurements. The adopted procedure equals an
244 AF decay rate of ca. 67 μ T/half-cycle and results in the highest ARM intensity achievable with the
245 employed instrumental setting and management software (Sagnotti et al., 2003; Sagnotti, 2003). The
246 ARM was then measured and stepwise AF demagnetized using the procedure applied to the NRM.
247 From the AF demagnetization data of both the NRM and the ARM we computed the median
248 destructive field (MDF), which is defined as the value of the peak AF necessary to reduce the
249 remanence intensity to half of its initial value.

250

251 The raw magnetic moment data measured by the three orthogonal SQUID sensors of the SRM
252 system were automatically corrected by compensating for the different shape and widths of the
253 response function curves of the three SQUID pick-up coils (Roberts, 2006). Moreover, we took
254 particular care in avoiding eventual disturbance effects that may be introduced during the coring,
255 cutting and sampling procedures and could result in remanence deflections due to plastic
256 deformation of the soft sediments. We also disregarded the paleomagnetic data for ~5 cm at both
257 ends of each u-channel to avoid disturbances linked to edge effects.

258

259 3.4 ²¹⁰Pb, ¹³⁷CS, and ¹⁴C AMS radiocarbon analysis

260 Continuous 1-cm³ samples were taken from the full length of the surface core (LUN12-2C), freeze
261 dried and sent to Flett Research Ltd. for ²¹⁰Pb and ¹³⁷CS analysis. Plant macrofossils for ¹⁴C AMS
262 dating were not found during the initial core description, therefore extensive efforts were made to
263 obtain datable materials. To find plant macrofossils and macroscopic charcoal, we sieved a total of
264 525 cm of core (90 samples, 5 from LUN09 and 85 from LUN12). For LUN09 we subsampled 20-cm
265 long sections of half the core (~200 cm³ per sample), soaked the sediments in a 5% solution of
266 sodium metaphosphate for 12 hours, then sieved at 250 μm. We followed the same process for
267 LUN12 but decreased the sample size to 5-cm long sections (~50 cm³). Two microscopic charcoal
268 samples were picked by hand from samples that appeared to be richer in charcoal. We concentrated
269 pollen from a 20 cm section of core for ¹⁴C AMS dating, following Newnham et al. (2007) then
270 separated the concentrate using flow cytometry (Tennant et al., 2013).

271

272 One macrofossil (LTL 4680A) was submitted for AMS analysis at CEDAD at the University of Salento,
273 Brindisi, Italy; all others were submitted to the Center for Accelerator Mass Spectrometry (CAMS) at
274 Lawrence Livermore National Laboratory, USA. All macrofossils were chemically pretreated with the
275 standard acid-base-acid (ABA) treatment before being combusted under vacuum and graphitized
276 according to standard procedures (Vogel et al., 1984).

277
278 A *Phragmites* plant growing in the lake was uprooted and pieces of the roots, stem, and leaves were
279 rinsed in deionized water before transport to LLNL for radiocarbon analysis. All samples were
280 pretreated, graphitized, and measured according to the same protocols as the fossil samples; dates
281 on the roots and leaves were replicated.

282

283 3.5 Tephra analysis

284 Italy has a history of active volcanic eruptions, although most are well to the south of our site and no
285 tephra from the last three millennia have been confirmed for our region (Giaccio et al., 2009;
286 Sulpizio et al., 2014). Nevertheless, to test the potential for tephrochronology, twelve 10 – 40 cm
287 thick samples were collected from LUN12-1B at age intervals, based on the paleomagnetic secular
288 variation age model, discussed below, corresponding to periods of eruptions from Vesuvius,
289 Phlegrean Fields, Ischia Island, Vulcano and the Lipari Islands. Eight samples were prepared on alloy
290 stubs for morphological and textural observations and qualitative chemical analysis of components
291 using a Zeiss EVO MA 10 scanning electron microscope (SEM) equipped with an Oxford ISIS
292 microanalysis system at INGV in Pisa. No tephra were recovered and this line of investigation was
293 not pursued further.

294

295 3.6 Pollen and charcoal analysis

296 A total of one hundred samples (0.625 cc volume) were processed for pollen analysis using acid
297 digestion procedures (Faegri and Iversen, 1985); two samples from the surface core (LUN12-2C),
298 forty from LUN09 (40-605 cm depth), and fifty-eight from LUN12-2B (460-1438 cm depth). A known
299 quantity of an exotic tracer (*Lycopodium*) was added to each sample during processing (Stockmarr,
300 1971) and counted along with pollen for calculating pollen concentration. Pollen counts for LUN09 (6
301 m in length) were completed before recovering LUN12-2B (14.4 m in length), therefore we counted
302 duplicate samples from each core for the overlapping section from 460 – 605 cm depth. Duplicate

303 counts were similar, and in the overlapping section we used only the counts from LUN12-2B, which
304 were done at a later date, for a total of ninety-one samples in the final pollen diagram. A minimum
305 of 400 terrestrial pollen grains were counted per sample (mean = 441) except for samples with very
306 low concentration rates (n = 23), in which case a sum of 200 – 300 grains were counted (mean =
307 222). Pollen count totals excluded aquatic pollen types, such as *Typha*, *Nuphar* and *Potamogeton*,
308 algae, and non-pollen palynomorphs.

309

310 Pollen and non-pollen palynomorphs were identified using reference material in the Tuscia
311 University Paleocology Lab, published keys and manuscripts (Punt and Malotaux, 1984; Punt et al.,
312 1991; Chester and Raine, 2001; Blackmore et al., 2003; Beug, 2004; van Geel and Aptroot, 2006;
313 Cugny et al., 2010; van Geel et al., 2011). TC pollen (Taxaceae and Cupressaceae) was assumed to be
314 *Juniperus*, a native taxa. Species of *Quercus* were identified as either *Q. pubescens - robur* L.type, or
315 *Q. cerris* L. (deciduous) or *Q. ilex* L.(evergreen) following van Benthem et al. (1984). For plotting
316 purposes *Quercus* is represented as deciduous or evergreen (*Q. ilex* type). Members of the family
317 Poaceae were identified as cereals if grains were >37 µm, pore diameter was > 2.7 µm and annulus
318 thickness was > 2.0 µm, following Köhler and Lange (1979). Pollen percentages were calculated from
319 the sum of terrestrial pollen, excluding indeterminate grains and *Cannabis* type (which was retted in
320 the lake at certain periods; Poni and Fronzoni, 2005). Accumulation rates (grains cm⁻² yr⁻¹) were
321 calculated by dividing concentration (grains cm⁻³) by the number of years per sample (yr cm⁻¹).
322 Aquatic taxa, algae, and non-pollen palynomorphs are presented as accumulation rates, since they
323 appear intermittently in the record and total quantity better represents actual abundance than does
324 percentage. Zonation was interpreted from a constrained single-link dendrogram created using
325 CONISS in the PolPal plotting program (Nalepka and Walanus, 2003). Data input included the fifty-
326 three terrestrial taxa with at least one strata of >1% of the pollen sum, excluding *Cannabis* type and
327 indeterminate grains.

328

329 Charcoal particles were counted on pollen slides in two size fractions, 50-125 μm and $>125 \mu\text{m}$ –
 330 longest dimension (Sadori and Giardini, 2007). All fragments that met the criteria of being black and
 331 having a visible cellular structure were counted.

332

333 3.7 Archaeological, Historical and Archival documents

334 The bulk of the archaeological documentation is represented by two surveys carried out in the area
 335 in the 1980s by the University of Perugia and in the 1990s by the British School at Rome (Coccia et
 336 Al., 1992; 1995).

337

338 The early medieval phase is well documented by one of the most important collections of Europe:
 339 the archive of the Farfa Abbey, which contains a body of documents concerning the history of the
 340 territory between the 8th and the 12th century AD. The late medieval phase (13th – 15th century) is
 341 well documented through the archive of the Comune of Rieti and that of Rieti cathedral (Caciorgna
 342 1998; 2000; Leggio 1998). The history from 16th century onward has been analyzed in detail by
 343 means of additional archive (Dupré, 1939; Lorenzetti 1989) and map collections in the Archivio di
 344 Stato in Rome and Rieti (Lorenzetti, 1990; 1994; 2009). In correlating the sedimentary evidence with
 345 historical evidence we have provided names and time periods following the system developed by
 346 Coccia et al. (1995) based on changes in archeologic ceramics in the Rieti Basin.

347

348 4. Results and Discussion

349 4.1 Chronology

350 Developing a core chronology based largely on ^{14}C dating, proved challenging given that the
 351 carbonate system appears to have imparted significant old-carbon effects and plant macrofossils
 352 were hard to find and not well-distributed throughout the core. We developed two independent age
 353 models, one based on historical documentation of biostratigraphic markers along with
 354 paleomagnetic secular variation (PSV) and another based on ^{14}C analyses (Table 1, Fig. 4). For both

ha eliminato: b

ha formattato: Apice

ha eliminato: produced

ha eliminato: radiometric (^{210}Pb and

ha eliminato:)

359 [age models, ²¹⁰Pb was used to provide the uppermost chronostratigraphic datum for both age](#)
360 [models.](#)

361

362 4.1.1 Biostratigraphic markers

363 Historical documentation of specific biotic changes within the basin (biostratigraphic markers we
364 refer to as cultigens) were compared with the pollen reconstruction to provide estimated dates in
365 the upper section of the core. *Zea mays* (corn) was introduced into Europe only after the first voyage
366 of Columbus in 1492 CE. The first historical documents noting cultivation of *Zea mays* in Italy are
367 from 1605 CE (Massafra, 1981) and most documents indicate that cultivation was initially sparse,
368 introduced into central Italy after 1700 (Messadaglia 1932). The first documented planting of *Zea*
369 *mays* in the Rieti Basin is given as between 1740 and 1760 CE (De Felice, R., 1965; Covino, 1995) and
370 we attribute a date of 1750 CE to the core depth (134 cm) with the first appearance of *Zea* pollen
371 (Table 2)

372

373 *Cannabis* cultivation in the Rieti Basin for rope production expanded in the mid-17th century peaked
374 in the late 18th century and eventually declined by the mid-19th century (Galli, 1840; Zuccagni-
375 Orlandini, 1843; Nigrisoli 1857; Celetti, 2007). The peak in Cannabis-type pollen (see Results Fig. 12)
376 is coincident with the first appearance of *Zea* pollen. We designated a date of 1660 CE to the
377 beginning of the rise in Cannabis-type pollen (160 cm) , and a date of 1830 CE to the end (110 cm), a
378 time when cheap cotton production began replacing *Cannabis* across Europe (Lavrieux et al., 2013).

379

380 Reforestation associated with land abandonment following the black plague in 1349 CE depth has
381 been documented repeatedly throughout Europe (van Hoof 2006; Yeloff and van Geel, 2007; Fraser,
382 2010; Sköld et al., 2010). Written documents from Rieti described a similar pattern of land
383 abandonment and reforestation towards the end of the 14th century (Leggio, 1995b; Naspi, 2010)

384 and we gave a date of 1390 CE to the major transition from a deforested to forested landscape
385 evident in the pollen record about 335 cm depth.

386

387 *4.1.2 Paleomagnetic analysis*

388 The measured rock magnetic properties (κ , NRM, ARM, MDF) were used to correlate cores LUN12
389 1A, 1B, 2A, 2B, 2C and LUN09 between overlapping sections and enabled us to build a composite
390 magnetic section for the lake (Fig. 5). We constructed an age model based on the rock magnetic data
391 and biostratigraphic cultigens described above

392

393 The NRM demagnetization data allowed the unambiguous identification of a Characteristic
394 Remanent Magnetization (ChRM) throughout all the sequence. The data indicate that the whole
395 sequence is characterized by an almost single-component NRM, unambiguously isolated after
396 removal of a weak viscous overprint in AF steps of 5-10 mT (Fig. 6). The orientation of the ChRM was
397 defined by principal component analysis (Kirschvink, 1980) by fitting a line between the 10 and 50
398 mT AF demagnetization steps. The maximum angular deviation for each determined ChRM direction
399 is 1° on average, with a full range of variation between 0.1° and 5°. The MDF of the NRM typically
400 ranges between 15 and 40 mT indicating that magnetite is the main magnetic carrier in the
401 sequence.

402

403 The ChRM declination of individual u-channels was arbitrarily rotated to align trends between
404 adjacent sections. The stratigraphic trends in the ChRM declination and inclination are characterized
405 by wide oscillations at high-frequency around the expected values for a geocentric axial dipole (GAD)
406 field at the site. These wide oscillations are however unexpected considering the observations and
407 the models of paleosecular variation (PSV) of the geomagnetic field over the last millennia (Gallet et
408 al., 2002; Pavón-Carrasco et al., 2009; Korte et al., 2011). In any case, these variations are consistent

409 between the analyzed cores and the reconstructed ChRM directional trends are replicated in the
410 overlapping sections of the distinct cores (Fig. 6).

411
412 To estimate relative paleointensity (RPI) variation, we normalized the NRM by κ and by the ARM
413 intensity. The NRM/ARM ratio was computed also from the values measured after the 20 mT and 40
414 mT AF steps. All the normalization methods resulted in a similar pattern and therefore support a
415 general coherency between the different normalization procedures and indicate a reliable
416 reconstruction of the RPI trend. After removal of data affected by edge effects at the u-channel
417 breaks, lithological boundaries and δ spikes, the broadly smoothed paleomagnetic trends can be
418 correlated to the available PSV curves and models for Europe (Gallet et al., 2002; Pavón-Carrasco et
419 al., 2009) (Fig. 6). This correlation enabled us to point out various depth-age tie-points from
420 prominent PSV features.

421
422 In order to estimate the temporal error of the paleomagnetic tie-points we have calculated the
423 temporal resolution of the regional model SCHA.DIF.3k at the geographic coordinates of Lago Lungo.
424 For each tie-point, the three geomagnetic field elements, i.e. declination, inclination, and intensity,
425 are defined by a temporal Probability Density Function (PDF). The PDF depends on the value of the
426 geomagnetic field element at the corresponding time and its uncertainty (the α_{95} in the case of the
427 directional elements and the intensity standard deviation, σ_F , for the intensities). The combination of
428 the three PDFs for each geomagnetic element provides a final PDF which area allows us to calculate
429 the minimum and maximum time for each tie-point. Then, the temporal resolution of the regional
430 model is given by the difference of this maximum and minimum. Table 1 contains the paleomagnetic
431 tie-points used in this study with the geomagnetic field elements and their uncertainties, at 95%
432 confidence levels, according to the SCHA.DIF.3k model predictions (Pavón-Carrasco et al., 2009).

433

434 *4.1.3. ^{210}Pb , ^{137}CS , and ^{14}C AMS radiocarbon analysis*

435 CS-137 activity was significantly above background for the core interval 24-41 cm with maximum
436 activity at 28-29 cm depth, assumed to be 1963 CE. The CRS model of ^{210}Pb activity indicated an age
437 of 1954 CE at 33.5 cm depth, and it was concluded that the CRS model provided a reasonable
438 estimate of age in this core. The ^{210}Pb chronology produced a date of 1905 CE at 50.5 cm depth and
439 provides an upper constraint for the top of both the PSV and ^{14}C based age models..

ha eliminato: s

ha formattato: Apice

440
441 Fifteen radiocarbon dates were obtained from twelve depths in the LUN09 and LUN12-1B cores
442 (Table 1 and Fig. 4). Sieving yielded six plant macrofossils and two macroscopic charcoal samples; all
443 remaining plant macrofossils and microscopic charcoal were found during the sub-sampling process.
444 Sorting of pollen by flow cytometry yielded 1.5 million pollen grains which were divided into two
445 samples (900,000 and 600,000) to obtain replicate dates for the interval 172-202 cm in LUN09. The
446 same interval yielded a sample of leaf fragments large enough to produce replicate radiocarbon
447 dates. The leaf replicates produced essentially identical radiocarbon ages, but were significantly
448 younger than the pollen replicates, by ~400 years. The pollen replicates are likely older because they
449 integrate grains from the whole 30 cm sediment sample, whereas the leaves may represent a single
450 depth of younger age.

451
452 The radiocarbon samples generally fit into two categories, based on their age and depth in the core.
453 Between 1000-260 cm four samples have calibrated radiocarbon ages of ~2800 years cal BP, with a
454 fifth (343 cm) dating to 3500 cal yr BP. Because of the similarity in age, despite a wide stratigraphic
455 range, and the variety of materials (Table 2), it seems likely that these samples represent the
456 occasional tapping of some remnant deposit formed at or before 2800 yr BP.

457
458 The second group of samples (n = 10) cluster between 266 and 159 cm, and produce radiocarbon
459 ages ranging from 1800 to 780 cal yr BP. This second group also represents a wide range of sample
460 types, and may be the result of a period of widespread and active erosion, caused by wetter overall

462 climate or more intensive human disturbance of the landscape, or both. The two groups of dates
463 overlap at ~260 cm depth.

464

465 We considered the relatively fragile uncharred leaf macrofossil ^{14}C dates (Table 1) the most reliable
466 upon which to develop a radiometric chronology (Hatté and Jull, 2007). Although we were unable to
467 identify leaf fragments to species, all appeared to be terrestrial. Macrofossils from core LUN-12 were
468 considered more reliable than those from LUN-09 because they were recovered from 5-cm thick
469 sections rather than 20 cm-thick sections. Since the sections from each core overlapped
470 stratigraphically, we used the ^{14}C dates from leaf macrofossils in LUN-12 (Table 1, samples with
471 center depths of 166, 193.5, 213.5, 238.5, 268.5, and 998.5 cm) to build an alternative age model.

472

473 4.1.4 Age model selection

474 To directly compare the two age models, we replotted the LUN-12 PSV data using the radiometric
475 dates as tie points (Fig. 8), and compared this fit with the available PSV curves and models for
476 Europe (Gallet et al., 2002; Pavón-Carrasco et al., 2009). Comparison of the two age models shows
477 that the ^{14}C based age model (Fig. 8) produces a poor fit between the LUN-12 PSV data and the PSV
478 curves and models for Europe, especially when compared with the age model based on
479 biostratigraphic markers and PSV tie points (Fig. 7). Note that each age model spans 3000 years,
480 however in the ^{14}C based model 3000 yr BP is at 10 m depth and in the PSV model this is at 14.4 m
481 depth. The ^{14}C based age model also produces age-depth relationships that are inconsistent with the
482 written history. For example, the ^{14}C based age model gives a date of 1380 CE for the depth of 134
483 cm, the first occurrence of *Zea mays* pollen, a physical impossibility given the introduction history of
484 that crop. The ^{14}C age model also results in dramatic changes in sedimentation rates at 268 cm
485 depth from 6.92 to 0.96 mm yr⁻¹. Although this is physically possible, there is no indication in the
486 appearance of the sediments (Fig. 3), or the geochemistry (Fig. 10) to support such a change at this
487 depth. Down core, further issues in interpreting the data emerge, including deforestation and

ha eliminato: in addition to the ^{210}Pb date (from 50.5 cm)

489 draining of the basin by 400 BCE, more than a century before archaeological and written records
490 suggest any Roman impacts.

491
492 Given the problems associated with the ^{14}C based age model, we conclude that the PSV age model
493 produces the most accurate chronology. In the PSV model, all three measures of paleomagnetism
494 (inclination, declination and intensity) can be tied to the European PSV model through the full length
495 of the core (Fig. 7), sedimentation rates do not change abruptly (Fig. 4), and the pollen record is
496 consistent with known history. In contrast, most of the ^{14}C ages fall within only one meter of the
497 core, with a 7m gap between the cluster of dates near the top and the only macrofossil found down
498 core. The clustering of macrofossils argues for the potential that macrofossils were transported to
499 the lake irregularly, perhaps during a wet phase through flooding, erosion and redeposition of old
500 materials. We do not have a complete explanation for the unusual ^{14}C dates, but in trying to
501 understand this problem we radiocarbon dated different parts of a single *Phragmites* plant growing
502 in the lake. This plant produced modern ^{14}C dates in the roots and leaves, but a date of >500 cal yr
503 BP from the stem (Table 1). Terrestrial plants that can grow in standing water (e.g. *Salix*) generally
504 produce reliable ^{14}C dates (Hatté and Jull, 2007). We intend to further explore the complexities of ^{14}C
505 production and uptake within the study area.

506

507 4.2 Geochemical proxies

508 Several elements (Ca, Sr, Ti, Fe, Mn, and S) serve as proxies for siliclastic input, and authigenic or
509 endogenic mineral fractions. The relationship of these elements can be seen in biplots of Principal
510 Components 1 and 2 (Fig. 9), where the eigenvectors (red arrows) of the elements are superimposed
511 over the data points, and 3 eigenvector trajectories (numbered 1, 2, and 3) are interpreted to have
512 sedimentologic significance. The Medieval Period (MP) and Little Ice Age (LIA) intervals are plotted
513 separately to show changes in elemental behavior between these two intervals (Figs. 9a, b). Ca is
514 representative of the calcium carbonate (CaCO_3) component of the sediments, indicated by the good

515 correlation between the Ca XRF and percent CaCO₃ derived from LOI (Fig. 10), and shows a distinct
516 separate trajectory on the PCA plots (Fig. 9). Sr can co-precipitate with Ca as SrCO₃ when the lake
517 waters are saturated with CO₃ (Haenssler et al., 2013), seen in the profile when Sr and Ca track
518 together. Sr can also behave conservatively as a detrital element, tracking closely with Ti (Kylander
519 et al., 2011). Ti is used in this study as a proxy for siliclastic detrital input into the lake (Haberzetti et
520 al., 2008), controlled by erosion, weathering, and runoff within the catchment. Ti is representative of
521 other conservative clastic elements such as K, Rb, and Zr that have near-identical profiles throughout
522 the core, and are seen to have near identical eigenvectors with Ti (Fig. 9). Fe, while at times also
523 behaving as a detrital element (Fig. 9b), is also influenced by redox processes and subject to
524 remobilization at the sediment-water interface (Croudace et al., 2006). Mn is also influenced by
525 redox processes, forming highly insoluble oxides in oxygenated conditions (Kylander et al., 2011) and
526 is used here as an indication of changes in redox behavior of the upper few cm of the sediment. Mn
527 shows a distinct trajectory in the PCA biplots, where Fe follows the behavior of Mn most closely in
528 the MP (Fig. 9a). Sulphur shows an interesting profile and has been used as an indicator of
529 evaporative balance and lake level changes, as it precipitates in chemically concentrated lake waters
530 (Haenssler et al., 2013).

531

532 *4.3 Core stratigraphy*

533 Core stratigraphy is delineated by gross sedimentologic characteristics that are supplemented with
534 petrographic observations, time series curves of κ and geochemistry. The sequence is subdivided
535 into four stratigraphic intervals that are assigned names based on their chronostratigraphic
536 significance. The sedimentology of these intervals is described below.

537

538 *4.3.1 Archaic through Early Medieval interval: 1438 - 800cm, Age: 700 BCE - 870 CE*

539 This interval represents a number of historical periods (Coccia et al., 1995); including the Archaic
540 (700 – 500 BCE), pre-Roman (500-300 BCE), Roman (300 BCE – 400 CE), Late Antique (400 – 600 CE),

541 and Early Medieval (600 – 800 CE) periods. Sedimentologically, the interval consists of a dark,
542 discontinuously laminated, silty to clayey marl. The color is dark gray to black and fades to an olive
543 color within hours of being exposed to air, indicating the presence of unstable monosulfides, or
544 other redox-sensitive minerals in a reduced state. Small (< 1mm) black streaks in the core are
545 aggregates of sub-micron-sized opaque black minerals within a clay matrix. Microscopic examination
546 shows that the carbonate phase is significant ($\geq 50\%$) in the form of calcite rhombohedrons (ranging
547 from 2-20 μm), detrital carbonate allochems (<5 μm), *Phacotus* algal grains (5-10 μm), and rare
548 fragments of Charophyte algae (>10 μm). The silt fraction is largely quartzofeldspathic, subangular,
549 and occurs throughout, becoming an increasingly larger component towards the top of this interval.
550 There is a diatom component (estimated at <10%) consisting predominantly of *cyclotelloid*
551 phytoplankton with smaller amounts of araphid periphyton.

552
553 Some trends are observed in the lower and upper portions of this interval. At the base, the
554 carbonate component is highest in the core and shows a gradual decline until 1250 cm (~300 BCE).
555 This is indicated in both a decrease in Ca counts and $\% \text{CaCO}_3$ determined by LOI, with a proportional
556 increase in siliclastic components, as seen in the counts of Ti and Fe (Fig. 10). The κ has a baseline of
557 $\sim 10\text{E}^{-5}$ SI, at the bottom of the core, then increases to $\sim 20\text{E}^{-5}$ sl, at 1150 cm reciprocating the
558 decreased carbonate fraction. Sediment accumulation rates decrease with the drop in carbonate
559 from $\sim 7 \text{ mm yr}^{-1}$ to the lowest rate in the core ($\sim 3 \text{ mm yr}^{-1}$). The top $\sim 1\text{m}$ of this interval, during the
560 Early Medieval Period (875-800cm; $\sim 800\text{-}900$ CE), shows some interesting sedimentologic and
561 geochemical features, although the distinction from the sediment below is not readily seen
562 macroscopically in the core photos (Fig. 3). The κ signal shows large, frequent peaks above 100 SI.
563 (Fig. 10), sediment accumulation rate rapidly increases to $\sim 12 \text{ mm yr}^{-1}$ and there is a brief increase in
564 carbonate content relative to siliciclastics. The uppermost ~ 45 cm, above 815 cm (870 CE), shows a
565 large elemental shift commensurate with a decrease in organic matter and carbonate content.
566 Diatoms are absent above 815 cm.

567

568 *4.3.2 Medieval interval: 800 - 335 cm, Age: 870 - 1390 CE*

569 This interval consists of gray thin bedded clay and silty-clay bands 1-30 mm thick, intercalated with
570 varicolored reddish-brown, black, and buff-colored bands 2 -10 mm thick. The reddish-brown to
571 black layers appear to be rich in Fe and Mn, based on alignment of the core photos to the scanning
572 XRF signal (Figs. 3 and 10). Fe and Mn show a close correspondence in the MP and have a similar
573 eigenvector trajectory (Fig. 9a). The buff layers are 2-12 mm thick carbonate-rich bands that locally
574 are hard and concretionary. Fine silty sand bands, 5-20 mm thick are interspersed throughout this
575 interval, and contain as much as 80% quartzo-feldspathic grains. The carbonate fraction consists of
576 small rhombohedrons, (2-5 μm), small detrital allochems (2-5 μm), *Phacodus* fragments (5-10 μm),
577 and Charophyte fragments (10-80 μm). Sediment accumulation rates are high, a result of increased
578 siliciclastic input, with correspondingly lower organic matter and carbonate fractions than the
579 preceding interval. Diatoms are absent from this entire interval, with the exception of very rare
580 fragmented or corroded frustules. The trends of the major elements, which shift dramatically at a
581 core depth of 815 cm, persist throughout this interval. The top of this interval is marked by a very
582 large κ peak not seen in the elemental data and a drop in sediment accumulation rate (Fig. 10).

583

584 *4.3.3 Early Modern - Modern: 335 - 140 cm, Age: 1390 - 1740 CE*

585 At a depth of 335 cm, the sedimentologic character shifts markedly. Siliciclastic content declines
586 rapidly and then becomes variable, dominated by organic-rich calcareous material containing
587 gastropod fragments and diatoms. Much of the organic matter appears to be aquatic in origin.
588 Within this interval are two light yellowish zones rich in thin carbonate stringers and lenticular
589 concretions. Petrographically, the carbonate is largely dendritic and ascicular, and of unknown
590 genesis. A subordinate fraction of the carbonate is definitively algal, composed of Charophyte and
591 *Phacodus* grains. Chemically, counts of siliciclastic elements (i.e. Ti) in this interval are the lowest in
592 the core, and Ca and Sr have several maxima (Fig. 10). Mn and Fe are decoupled throughout this

593 interval, and large peaks in S are observed for the first time, concurrent with none of the other
594 elements. The organic matter content is the highest throughout the core, following trends in both Ca
595 and Sr.

596

597 *4.3.4 Late Modern to Contemporary interval 0-140 cm, Age: 1740 to 2000*

598 This interval is composed of mottled and homogeneous to discontinuously laminated gray-black-
599 marl. The gray color appears to be related to carbonate content, with the lighter bands showing a
600 higher percentage of carbonate grains. Diatoms are common as is aquatic organic matter. The
601 carbonate fraction is more heterogeneous than lower intervals, and is composed of a mix of calcite
602 rhombohedra, detrital allochems, *Phacodus*, and subordinate amounts of dendritic grains. There is a
603 clay-sized siliclastic component, containing small amounts of fine (2-5 μm) silt grains.

604

605 *4.4 Pollen, non-pollen palynomorphs and charcoal*

606 We identified ninety different pollen types, nine non-pollen palynomorphs and eleven algae types.
607 Pollen taxa with percentages consistently >1% are presented for trees (Fig. 11) and herbs (Fig. 12)
608 and for the most abundant aquatic pollen, algae, and non-pollen palynomorphs (Fig. 13). Dominant
609 taxa and percentages are summarized in Table 3.

610

611 Five pollen zones were interpreted from the dendrogram. Zone 1 (1438 – 1145 cm; 700 BCE to 1 CE)
612 includes the Archaic, pre-Roman and Roman republican periods (Coccia et al., 1992). Zone 2 has
613 been divided into two subzones; Zone 2A (2A, 1145 – 970 cm; 1 CE to 600 CE) corresponds to the
614 Roman Imperial period through Late Antique period, and Zone 2B (970 – 800 cm; 600 to 870 CE)
615 corresponds to the Early Medieval period. Zone 3 (800 – 335 cm; 870 to 1390 CE), corresponds to
616 Medieval through Late Medieval time, Zone 4 (335 – 140 cm 1390 to 1730 CE) corresponds to the
617 Early Modern and Modern periods, and Zone 5 (140 – 0 cm; 1730 CE to present) corresponds to the
618 late Modern through Contemporary periods.

619

620 *4.5 Interpretation of Major Phases of Environmental Change*

621 There is a strong coupling between sedimentological and palynological shifts indicating that the
622 factors affecting the lake's depositional environment were also at work affecting the plant cover in
623 the surrounding landscape. The resolution of our age model is centennial to sub-centennial and
624 allows us to identify the major shifts in environmental change to compare with the rich collection of
625 archeological and archival evidence and independent climatic reconstructions. The record allows for
626 recognition of distinct periods or phases within the last 2700 years. Here we discuss the seven most
627 important environmental phases in a historical context and the potential climatic and human causes
628 that may have caused those changes.

629

630 *4.5.1 Pre-Roman: A climate driven system (700 – 300 BCE)*

631 Environmental change during the pre-Roman period appears to be largely a response to climate
632 rather than human activity. The climate was cool and wet at the beginning of our record. The
633 Calderone glacier, 50 km to the east in the Gran Sasso d'Italia mountain group, advanced between
634 900 and 750 BCE and periglacial soils are found in the Apennines during the same period (Giraudi,
635 2005; Giraudi et al., 2011). Archaeological excavations and surveys from near Lago Lungo reveal
636 small settlements along the 375 m contour, suggesting habitation in a generally marshy environment
637 around small lakes (Coccia et al., 1995). The Sabini, who inhabited the region, were an advanced
638 culture and primarily exploited the land for pastoralism with little evidence of forest modification.
639 (Cifani, 2003). The literary tradition reports that in the Rieti Basin the cults of Vacuna and Hercules
640 played an important role, the first as the deity of water and woods and the latter the god of springs
641 and cattle (Alvino and Leggio, 2006; Camerieri, 2011).

642

643 There was a well-developed floodplain forest (*Alnus glutinosa* and *Fraxinus excelsior*) probably
644 covering much of the basin floor and lakeshore and a rich mesophyllous forest (*Fagus*, deciduous

645 and evergreen *Quercus*, *Ulmus*, *Carpinus betulus*, *Acer*, and *Corylus*) on the uplands (Fig. 14). The
646 abundance of *Fagus* pollen, and the presence of *Asterosporium*, a spore associated with *Fagus*,
647 suggests that beech forests grew on the lower mountain slopes well below 1000 m, while today they
648 are restricted above 900-1000 m (Piovesan et al., 2005). The mix of tree species as well as monolet
649 and trilete ferns (e.g. *Osmundo-Alnion* and *Alno-Ulmion* alliances; Cutini et al., 2010) supports an
650 interpretation of a minimally impacted forest (Russo Ermolli et al. in press). This widespread mixed
651 floodplain mesophyllous forest confirms that the landscape ecology of Central Italy was less affected
652 by the Mid Holocene 'mediterraneanization' than other southern regions of the Mediterranean
653 basin (Sadori et al., 2011).

654

655 The maximum highstand of *Lacus Velinus*, determined by geomorphic and archeological evidence
656 (Ferrel et al., 1992), is reported to have occurred in the Iron Age (beginning ~850 BCE). The lake
657 environment was a hydrologically open hard-water system (Ferrel et al., 1990) deep enough to
658 support aquatic phytoplankton (i.e. cyclotelloid diatoms). Carbonate content and Ca relative
659 abundance show a gradual decline in Lago Lungo from 700 - 400 BCE. The sediment accumulation
660 rate during this period remains low, indicating that the decrease in carbonate is not due to dilution
661 by clastic input. Instead, the carbonate trend reflects a change in lake chemistry affecting carbonate
662 saturation and precipitation. The *Lacus Velinus* highstand reached an elevation of 375 m a.s.l., then
663 dropped to ~372 m a.s.l. during pre-Roman time (pre 270 BCE), prior to any human modifications to
664 the basin (Ferrel et al., 1990). The coincidence of a larger deeper lake in ~850 BCE, receding during
665 pre-Roman times from its highstand supports the role of the water balance in affecting the observed
666 carbonate trend. The gradual decline in carbonate content may reflect climatically-driven changes in
667 lake hydrochemistry, although the specific drivers affecting carbonate deposition in this system need
668 more investigation.

669

670 4.5.2 Roman Republican: Initial manipulation of the drainage system (300 – 1 BCE)

671 About 270 BCE, the Romans are purported to have created *Cava Curiana*, a drainage canal cut
672 through the travertine sill at the location of the Marmore Falls to facilitate drainage and reclamation
673 of the basin (Leggio and Serva, 1991). There is a κ spike at ~300 BCE as well as an inflection point in
674 many of the geochemical curves, including carbonate, TI and S, which may be associated with the
675 channel cutting. The sediment remains dark gray to black with anoxic sulfides similar to the Pre-
676 Roman core interval, and no discernible sedimentologic event accompanies the κ spike. However, if
677 channel cutting served to lower Lago Lungo and temporarily isolate it from the larger lake system,
678 then the subtle increases in the S signal seen above the κ spike may reflect a more isolated stagnant
679 lake with slightly more sulfidic mineralization. The steady decline in *Alnus* pollen beginning ~200 BCE
680 (Fig. 14) supports an interpretation of a lowered water table despite above average precipitation
681 (Büntgen et al., 2011); however, large areas of the valley must have remained wet given the
682 continued persistence of *Alnus*. The decline in *Alnus* was permanent, indicating that after this
683 change the basin never again reached the same extent of flooded forest. Pliny the Elder (*Naturalis*
684 *historia* 3, 109) described the Rieti basin as covered by dense forest and beyond the change in *Alnus*,
685 there is no evidence for forest degradation (Fig. 14).

686
687 *Alnus* requires standing water, and a reduction in *Alnus* suggests a reduction in wetland area in the
688 valley. This interpretation supports the argument that the Roman's first drained the Rieti Basin in the
689 first quarter of the 3rd century BCE, as recorded by historians (Sisani, 2009). This reclamation work
690 appears to have been sufficiently successful to have lowered the water table enough to reduce the
691 flooded forests. The Roman water works do not appear to have changed land use practices.
692 Archeological surveys indicate that local settlements were consolidated (Coccia et al., 1995) but in
693 the 1st century BCE Varro emphasized the importance of sheep pasturing (Varr. 2.2.9) and the
694 geographer Strabo described the Reate valley as a place of domestic livestock, mules particularly
695 (Strab. 5.3.1). The increase in disturbance taxa during this period supports an interpretation of
696 increased pasturage.

697

698 *4.5.3 Imperial Roman through Late Antique: Intensification of land use (1 – 600 CE)*

699 Climatically, the period from 1 – 200 CE is considered part of the Roman Optimum, with exceptional
700 climate stability and favorable conditions that coincide with the rise of Imperial Rome (McCormick et
701 al., 2012). Reconstructed temperatures during this period were mild (Fig. 14), similar to the first half
702 of the 20th century (Christiansen and Ljungqvist, 2012; northern hemisphere extratropical 2000
703 temperature reconstruction –
704 [ftp://ftp.ncdc.noaa.gov/pub/data/paleo/contributions_by_author/christiansen2012/christiansen201](ftp://ftp.ncdc.noaa.gov/pub/data/paleo/contributions_by_author/christiansen2012/christiansen2012.txt)
705 [2.txt](ftp://ftp.ncdc.noaa.gov/pub/data/paleo/contributions_by_author/christiansen2012/christiansen2012.txt) URL and data accessed). What is particularly striking is that while the population of Rome
706 expanded to more than one million (Lo Cascio and Malamina, 2005) there is no evidence for
707 intensive exploitation of the Rieti Basin through land clearance or deforestation. Forests declined
708 during the Imperial period in relation to the Republican period (66% vs. 81% total AP respectively;
709 Table 3, Fig. 14), though the extent of degradation appears limited. The impact on the forest shows
710 alternating phases of more pressure (1st and 4th century) or less 3rd century (see also Russo Ermolli et
711 al., 2014) consistent with the demographic and socio-economic trends of Rome (Leggio, 2000;
712 Costambeys, 2009).

713

714 There is an abrupt increase in disturbance species (e.g. *Rumex*, Brassicaceae, Cichorioideae,
715 Apiaceae, and trilete spores) although a diverse flooded forest assemblage persisted. Pollen of
716 cereals are present, but not abundant (Fig. 12) and *Sporormiella*, an indicator of domesticated
717 livestock, is consistently present. Archeological evidence of settlement is restricted to the alluvial
718 fans and low hill-slopes above the valley floor, concentrated between 380 and 480 m with no
719 evidence of large settlements above 600 m (Coccia et al., 1995). The main nucleated settlement was
720 Reate (Cifani 2003) and the economy was probably oriented towards pastoralism and trade with the
721 nearby Apennine communities. We infer that the basin was partially cleared for pasture but

722 remained marshy and that livestock grazing was more important than agriculture, although even
723 pasturage may not have been intensive.

724

725 A number of other pollen reconstructions from the Italian peninsula have also found only limited
726 evidence of deforestation during the Roman Imperial period, including sites near Naples (Russo
727 Ermolli and Di Pasquale, 2002) Colli Euganei west of Venice (Kaltenrieder et al., 2010), Calabria
728 (Joannin et al., 2012), Abruzzo (Branch and Marini, 2013) and near Ostia, the ancient port for Rome
729 (Di Rita et al., 2010; Sadori et al., 2011). Our findings contrast with arguments for extensive forest
730 clearing and burning in the vicinity of Rome (e.g. McNeil, 1992; Hughes, 2011) and support the
731 argument that deforestation was localized and degradation limited (Grove and Rackham, 2001).

732

733 The Roman Empire supported a complex trade network and one possible reason for the lack of
734 exploitation of the Rieti Basin may have been the 'globalization' of production of Imperial Rome.
735 Rieti was interconnected with Rome and likely benefited from external resources, potentially
736 reducing pressure on local resources (Champion, 1995). Local sites, such as Rieti, would not have
737 been sufficient to support the large urban population of Rome and may have been spared from
738 environmental degradation while distant regions were exploited. Egypt appears to have enjoyed
739 exceptionally favorable conditions between 1 and 200 CE (McCormick et al., 2012) and food
740 production and transport may have been more efficient from such distant locations as opposed to
741 local sites with limited agricultural capacity and barriers to transport. Rieti was on the Via Salaria,
742 one of the most important trans-Appennine roads between Rome and the Adriatic Sea (Coccia et al.,
743 1992), but the Marmore Falls prevent easy access by water to the Tiber River making it difficult to
744 ship bulky resources (e.g. wheat, charcoal) to Rome. Another possibility is that, in order to prevent
745 deforestation and soil erosion and to mitigate Tiber flooding in the area of *Lacus Velinus*, the forests
746 were provided some level of protection as sacred woods, following the Sabini cult of Vacuna,
747 identified as Vittoria or Diana by the Romans (Alvino and Leggio, 2006; Coccia et al., 1992).

748

749 Between 400 and 600 CE, during the Late Antique period, sometimes referred to as the Migration
750 Period, we see a further degradation of the forest with a decline in *Ostrya* and increase in grassland
751 (Poaceae), indicating more intensive coppicing of forests and possibly an intensification of local
752 resource extraction. The Late Antique or Migration Period (400-600 CE), a time with cooler than
753 average temperatures and general disruption following the Roman Empire (Büntgen et al., 2011;
754 Christiansen and Ljungqvist, 2012), is sometimes identified as a period of climatic instability which
755 may have contributed to cultural upheaval (McCormick et al., 2012). In Rieti, there are few
756 indications of upheaval, however trade networks appear to have been disrupted requiring greater
757 reliance on local products. With the fall of Rome, the Ostrogoths ruled Rieti between 400 and 570 CE
758 and maintained the Roman system of governance (Leggio, 1989b). Archaeological data support the
759 presence of a thriving community (Coccia et al., 1995). Archeological data point to limited ceramics
760 from this period, indicating a potential breakdown in the trade system (Coccia et al., 1992). A decline
761 in *Ostrya* and increase in disturbance taxa suggest possibly more intensive coppicing of forests and
762 an intensification of local resource extraction, with less reliance on traded goods.

763

764 4.5.4 Early Medieval: Intensification of forest disturbance and sedimentation (600 – 900 CE)

765 This phase represents a transition period with a complex series of changes in the vegetation,
766 sedimentary, magnetic and geochemical proxies. Between 600 and 735 CE temperatures in the
767 northern hemisphere remained cooler than average (Christiansen and Ljungqvist, 2012) though in
768 central Europe, climate became milder, with warming temperatures and an increase in precipitation
769 (Büntgen et al., 2011). At our site, loss of forest biodiversity began ~600 CE, particularly the softer
770 hardwoods (*Fagus*, *Tilia*, *Ulmus*, *Acer*, and *Fraxinus excelsior*) (Zone 2B, Fig. 11) and there was an
771 increase in disturbance taxa (Fig. 12) and erosion (*Glomus*, Fig. 13). High percentages of *Alnus*
772 indicate that the valley floor remained marshy, suggesting that human impacts were concentrated
773 on the hill slopes.

ha eliminato: l

775

776 A milder and wetter climate should not have resulted in loss of forest biodiversity and we suggest
777 that this environmental shift resulted from a change in the governing authority and associated
778 changes in land use. The Lombards gained control of Rieti around 590 CE (Naspi, 2010). There are
779 few written documents for this period, but Rieti has been described as changing from a city of stone
780 to a city of wood (Leggio, 2000) and between ~600 and 800 CE, the softer desirable hardwoods were
781 selectively removed initiating the decline in forest biodiversity (Fig. 11). In addition, the Farfa
782 Monastery of the Benedictine order, established in the end of the 6th century in the Sabini
783 Mountains (Fig. 1), became increasingly important in the 8th century. The monks were responsible
784 for managing large areas of the landscape, including the Rieti Basin (Leggio, 1994) and forest cutting
785 was widespread (Leggio and Serva, 1991).

786

787 From ~735 CE (900 cm depth) until ~870 CE (800cm depth) the forest recovers somewhat, with an
788 increase in *Quercus* and *Ostrya*, although there is no increase in the soft hardwoods. Disturbance
789 indicators decrease, Ti decreases, carbonate and Ca increase, and MS is high and variable. Written
790 sources describe an increase in flooded area, expansion of Lago Lungo (*lacus Totonni*) and Lago di
791 Ripasottile (*lago Maggiore*) and the formation of many *lammae* (little lakes) (Leggio 1994; 1998). This
792 would appear to be a climatic impact, rather than a human induced change, though dominance of
793 *Quercus* and *Ostrya* in the overstory suggests an actively coppiced forest.

794

795 4.5.5 Medieval through Late Medieval: Peak deforestation and sedimentation (900 – 1390 CE)

796 The most extensive degradation of the environment occurred during the Medieval Period (~870-
797 1390 CE) when forest cover was greatly reduced and herbs and ferns increased (Fig. 14).
798 Temperatures in the northern hemisphere began warming after 900 CE with a well-defined peak
799 between 950 and 1050 CE (Fig. 14) and a maximum temperature anomaly of 0.6 °C (Christiansen and
800 Ljungqvist, 2012). Climate reconstructions from the central eastern Alps (Büntgen et al., 2011) and

801 central Italy (Guiot and Corona, 2010) show elevated temperature from 700 to 1250 CE with a
802 thermal maximum of 0.3 °C between 1053 and 1171 CE (Trachsel et al, 2012). A precipitation
803 reconstruction (Palmer Drought Severity Index - PDSI) using *Cedrus atlantica* (Endl. Carrière) from
804 Morocco (Esper *et al.*, 2007; Trouet *et al.*, 2009) shows that the period from 1050 to 1400 CE was
805 anomalously dry across the western Mediterranean (Fig. 14). The initiation of forest cutting
806 throughout the Rieti Basin coincides with the period of warmest temperatures, and climate change
807 appears to have been a strong catalyst leading to environmental degradation; however
808 socioeconomic changes are also important during this period.

809
810 Sediment accumulation rates reach their highest levels. The high percentages of indeterminate
811 pollen (Fig. 12) as well as Cichorioideae, a taxon commonly found on disturbed sites with pollen
812 particularly resistant to degradation (Bottema, 1975), support an interpretation of high erosion and
813 increased bare soil. Some of the indeterminate pollen are likely degraded tree taxa, suggesting that
814 the level of deforestation may not have been as high as the pollen diagram indicates; however there
815 is no reason to believe that the percentage of indeterminate pollen are skewed towards tree types
816 since many herbaceous taxa are equally subject to degradation. Fern spores (trilete) are very high
817 between 925 and 1075 CE. Ferns require mineral soil for regeneration, further supporting an
818 interpretation that large areas with thin soils must have been present and loss of tree cover must
819 have been widespread. The elemental proxy for erosion, the detrital element Ti, remains high
820 throughout the MP, supporting the claim that deforestation and agricultural land use peaked during
821 this time. Sediments throughout this phase are varicolored silty and clayey bands (Fig. 3) indicative
822 of episodic sedimentation and potentially greater fluvial influence. The very high sediment
823 accumulation rates begin to decline after 1100 CE.

824
825 Written and archeological evidence support the hypothesis for a large increase in population,
826 leading to saturation of the lower elevation sites for agriculture, and a push to exploit higher

827 elevations. During the Medieval period, settlements were constructed at elevations above 1000 m
828 (Coccia et al., 1992). Terraced walls related to farming were found between 700 and 1000 m (Coccia
829 et al., 1995) and active deforestation and a series of 'hospitals' for tending to farm workers have
830 been documented at 1400 m (Naspi, 2010). It also seems reasonable to conclude that warmer
831 temperatures allowed farming and grazing to be successful at higher elevations. As population grew
832 and settlement expanded upslope, farmers likely pushed the limits of what local resources were
833 capable of supporting (Wood, 1998). Introduction of the heavy plough, horse collar and harrow were
834 technological innovations that partially offset the limits of local production by permitting a more
835 intensive agriculture (Sereni, 1973).

836

837 Documents record an increase in deaths due to malaria (Bruce-Chwatt and de Zulueta, 1980;
838 Sabbatani, 2005) which may have also contributed to building settlements at higher elevation
839 (Leggio, 1994). Settlement was not dispersed, but largely concentrated in fortified settlements or
840 castles (*incastellamento*) for security. More than forty settlements in the Rieti Basin are first
841 mentioned in the Farfa monastery documents in the period between 1050 and 1200 CE, of which
842 fifteen of these hill towns are still occupied (Coccia et al., 1992). Dispersed settlements did not
843 completely disappear, but the broad pattern was one of the population concentrated into fortified
844 settlements in defensible locations governed by powerful and wealthy lords (Leggio, personal
845 communication). A sharp decline and intermittent absence of *Alnus* from the record indicates that
846 the valley must have also been heavily managed and utilized for cereal production. Only through
847 constant maintenance of the drainage system was it possible to prevent the basin from becoming
848 marshland (Coccia et al., 1992). This maintenance was probably aided by a drier than normal climate
849 and large available labor force. A possible explanation for the new phase of exploitation of the valley
850 is that the slopes were not sufficient to maintain the needs of the increasing population (Naspi,
851 2010).

852

853 Following the MWP thermal maximum, the initial cooling of the LIA began, reaching a temperature
854 anomaly of $-0.8\text{ }^{\circ}\text{C}$ about 1310 CE (Fig. 14; Büntgen et al., 2011; Christiansen and Ljungqvist, 2012;
855 Trachsel et al., 2012). The black plague of 1347 CE, and subsequent famines and plagues resulted in
856 a local population decline of $>50\%$ by 1400 CE (Leggio, 1989b). Cooler than average temperatures
857 between 1350 and 1390 CE appear to have been a catalyst leading to collapse of the local land
858 management system. As high elevation settlements were abandoned (Leggio, 1995b; Naspi, 2010)
859 disturbance species decreased, and forest taxa and *Alnus* begin to steadily increase (Fig. 14).

860

861 *4.5.6 Little Ice Age: Rapid reforestation and reduced sedimentation (1390 – 1700 CE)*

862 A combination of climatic change, plague, earthquakes and political instability led to a collapse of
863 the local system by the early 15th century. Precipitation increased and temperatures remained cool
864 (Christiansen and Ljungqvist, 2012, Büntgen et al., 2011). Cooler wetter climate beginning in the 14th
865 century is supported by tree-ring and flood data. By ~ 1390 CE, the PDSI reconstruction from
866 Morocco records anomalously wet conditions, with peak wetness in the 15th and 16th centuries
867 (Esper et al., 2007). Records of major floods on the Tiber River through Rome began an upswing in
868 the 14th century and reached a maximum in the 15th century with a total of seventeen major floods,
869 an average of one every 6 years (Bersani and Bencivenga, 2001). In contrast, only three major floods
870 were recorded in the 13th century. San Matteo church documents and the 1445 CE Rieti cadastral
871 survey indicate that lakes in the basin reached their maximum extent during this period) Leggio,
872 2007).

873

874 The rock magnetic parameters (Fig. 5) indicate a significant event at the very end of the Medieval
875 interval (337 cm depth, ~ 1380 CE) followed immediately by changes in the geochemical data (Fig.
876 10) and representing a permanent change in the sedimentary dynamics in the lake. All clastic proxies
877 (κ , Ti, and smear-slide petrography) dropped to zero at 335 cm depth. Such a change required an
878 abrupt adjustment to the sedimentary environment, cutting off all access of siliciclastic input. This

879 shift coincided with a series of physical influences on the environment (strong earthquakes in central
880 Italy and increased precipitation) as well as socioeconomic influences (depopulation following the
881 Black Plague, local political instability). Historical documents of the second half of the 14th century
882 report difficulties in managing the drainage system of the basin and consequent famine (Leggio and
883 Serva, 1991). The geochemistry is very distinct with large peaks in Sr, S and Ca (Fig. 10) that are
884 indicative of changes in water chemistry and potentially a rearrangement of source waters to include
885 a more SO₄-rich source.

886

887 Increasingly cooler temperatures pushed people out of the highest elevation settlements, resulting
888 in widespread land abandonment (Leggio, 1995b; Naspi, 2010) and rapid recovery of forests.
889 Recurring plagues through the first half of the 16th century (Barbiera and Dalla Zuanna, 2009; Tozzi,
890 2009; Alfani, 2010) reduced the Italian population to its lowest level in Medieval time (Fig. 14) by the
891 mid-15th century (Capasso and Malanima, 2007). The peak in percent arboreal pollen and pollen
892 accumulation rate ~1600 CE coincides with the coolest temperatures during the LIA (Ladurie,
893 1971). This pattern of land abandonment and reforestation following demographic decline from the
894 black plague, and deterioration of the climate has been documented repeatedly throughout Europe
895 (van Hoof 2006; Yeloff and van Geel, 2007; Fraser, 2010). While the reforested phase in many
896 northern European sites lasted about a century, it lasted for two centuries in Italy. Political instability
897 and the persistent presence of mercenary bands made it increasingly unsafe to pasture livestock far
898 from settlements and hunting and fishing became increasingly important (Lorenzetti, 1989). By the
899 mid-15th century, the meat of deer and wild boar was less expensive than that of domesticated
900 animals and predators such as bears and wolves were present (Leggio, 1995a) providing evidence for
901 return of a functioning forest ecosystem. This pattern of the increased importance of game over
902 domesticated animals has been documented in France as well (Vecchio, 1974).

903

904 Despite extensive land clearing and erosion during the Medieval Period, forest cover was able to
905 quickly recover during the Little Ice Age (Fig. 14), although forest biodiversity did not return to the
906 level of the Roman and pre-Roman periods. One possible reason for the quick recovery may have
907 been associated with the practice of coppicing, in which, although dramatically thinned, stems
908 remain in the landscape and stem sprouts grow rapidly in the absence of repeated cutting. High
909 percentages of *Alnus* indicate that the basin must have been flooded through much of this period.
910 The lake expansion in the 15th century was so widespread in the basin that the 1445 CE cadaster
911 reported thirty-eight small lakes (Leggio and Serva, 1991); moreover in the historical maps of 1500-
912 1600 CE the flooded area is expanded, often reported as a single lake.

913

914 Tree crops, particularly *Olea* (olive) and *Juglans* (walnut), became more important after 1390 CE (Fig.
915 11). Around 1350 CE, a set of local regulations were codified governing the pruning and maintenance
916 of tree crops (Caprioli, 2008). During Medieval time, olives as well as walnut were not important
917 food crops in this interior area of the Sabina (Leggio, 1995b; Naspi, 2010) but after 1390 CE they
918 increased in abundance and became a larger proportion of the diet. Following an initial increase in
919 *Olea* pollen, there is a distinct decrease in abundance between ~1550 and 1650 CE. This is coincident
920 with an intense cold period documented throughout central and southern Europe, with the coldest
921 temperatures occurring in the late 16th and early 17th centuries (Ladurie, 1971; Trachsel et al., 2012;
922 Moriondo et al., 2013). At least seven different years with olive-killing frosts were recorded in
923 Provence, France between 1565 and 1600 CE (Ladurie, 1971). The Rieti basin is a marginal
924 environment for olives and the decline in pollen is likely attributable to repeated killing frosts.

925

926 After 1600 CE *Alnus* pollen shows a continuous and permanent decline providing evidence for a
927 lowering water table (Fig. 14) despite steady or increased precipitation (Büntgen et al., 2011; Esper
928 et al., 2007). Since the 13th century, many efforts had been made to construct new channels to
929 remove water from the basin, including the unnamed 1325 CE channel, *Cava Reatina* (1422 CE),

930 *Cava Paolina* (1547 CE) and *Cava Gregoriana* (1575 CE). These efforts were largely unsuccessful until
931 construction of *Cava Clementina* in 1601 CE (Lorenzetti, 1989; Leggio and Serva, 1991). Decline in
932 *Alnus* after 1600 CE appears to be a response to human activity rather than climate.

933

934 *4.5.7 Late Modern and Contemporary: Modern forest with lake eutrophication (1700 CE to present)*

935

936 By the 18th century, the vegetation structure was essentially modern. Drainage of the basin removed
937 all flooded forest and agriculture included introduced crops such as *Zea mays* (Fig. 11). *Cannabis*
938 type production peaked in the late 18th and early 19th centuries, with the very high pollen
939 percentages likely associated with retting in the lake (Poni and Fronzoni, 2005; Celetti, 2007). The
940 slopes remained forested but contained much less biodiversity than the original landscape, even
941 though pollen percentages suggest that total forest cover is not significantly less now than during
942 the pre-Roman period. The successional species *Juniperus communis* and *J. oxycedrus* are now an
943 important forest constituent whereas for most of the record it was a minor component of the
944 vegetation. The lakes appear to have become increasingly eutrophic with dramatic increases in
945 diatoms, soft-bodied algae and calcareous algae towards the present (Fig. 13). The intensity of
946 human impacts increased such that the human signal is much stronger than the climate signal of
947 environmental change.

948

949 **Conclusions**

950 Our 2700 year paleoenvironmental reconstruction on the fringes of Rome records a complex
951 interaction between climate and socioeconomic conditions as drivers of environmental change. The
952 influence of Rome on the Rieti Basin during the Roman Republican Period seems to be modest.
953 Despite the channel excavations that formed the falls at Marmore and drained the basin, our multi-
954 proxy record indicates that the effects on both the aquatic ecosystem and landscape were minimal.
955 During the Imperial Roman Period, a time of generally mild climate, referred to as the Roman

956 Optimum, although Rome reached one million inhabitants, there is no evidence for deforestation in
957 the Rieti Basin and only limited impact on the environment. The Roman Empire supported a complex
958 trade network that allowed importing resources from distant regions, similar to modern
959 globalization. Rieti was interconnected with Rome and likely benefited from external resources, and
960 reduced pressure on its local resources, resulting in preservation of the environment. With the fall of
961 Rome, despite a cooler climatic period associated with an interval of general disruption in central
962 Europe referred to as the Migration Period, the Ostrogoths filled the power vacuum in Rieti and
963 generally maintained an environment similar to that which existed during the Roman period. Only
964 with the arrival of the Lombards and establishment of local monasteries at the start of the Medieval
965 Period (~600 CE) did initiation of deforestation really begin, with clearing for agriculture and
966 selective removal of desirable tree species for housing and manufacture. This period is manifested in
967 a strong dramatic signal in the Lago Lungo record that transgresses all of the biological, geochemical,
968 and sedimentological proxies.

969
970 The climatically optimal Medieval Warm Period appears to have been a catalyst for expanded land
971 use and widespread environmental degradation. Local population was higher than during Roman
972 time, placing greater pressure on local resources, but another possibly crucial difference was the
973 lack of an interconnected trade network capable of supplementing local resources. As population
974 grew and settlement expanded upslope, they likely pushed the limits of what local resources were
975 capable of supporting. When a cooling trend began in the 13th century, the highest elevations began
976 to be abandoned and the forests began to recover somewhat. By the late 14th century, plague
977 devastated the local population. Persistent cooler and wetter climate led to wide scale land
978 abandonment and rapid reestablishment of the forest and wetlands. Climate change, coinciding
979 earthquakes produced marked changes in the local sedimentologic regime of Lago Lungo, including
980 diversion of siliclastic input and altered lake hydrochemistry. The Medieval period in Rieti has a
981 complex socioeconomic history, but the evidence supports the argument that the shift from warm

982 and mild climate to cool and wet climate was an important catalyst in disrupting the community.
983 This disruption lasted for nearly two centuries. By the 1600s, despite being one of the coldest
984 periods of the LIA, improved methods in hydrologic works led to the eventual permanent draining of
985 the basin and renewed agricultural expansion which has continued to today.

986

987 The Lago Lungo sediments are characterized by good paleomagnetic properties, with an almost
988 single-component ChRM that can be easily isolated with stepwise AF demagnetization. The ChRM
989 inclination and declination values oscillate around the mean values expected for the GAD field at the
990 site, but the amplitude and the frequency of the variation are too high for geomagnetic secular
991 variation. The paleomagnetic trends (ChRM inclination, declination and relative paleointensity) can
992 be replicated at high-resolution between four distinct cores, ruling out disturbance as a cause for
993 this variation. Regardless of the high-amplitude and high-frequency variation, when broadly
994 smoothed the reconstructed paleomagnetic trends can be correlated to the reference curves from
995 models of paleosecular variation (PSV) during the last 3000 years, as reconstructed from
996 archeomagnetic data collected across Europe. Together with constraints coming from pollen and
997 sediment analysis, the paleomagnetic trends allow the construction of a high-resolution age model
998 and indicate that some changes observed in the pollen assemblage and in sedimentation in the Rieti
999 basin can be associated to societal factors and others to climatic change. Paleomagnetism is a
1000 powerful tool for providing alternative age models for study sites with ^{14}C records that are difficult to
1001 interpret. The rich documentary record for the region provides an opportunity to further explore
1002 questions of environmental change in relation to societal versus climatic causes. Addressing some of
1003 these questions will require further refinement of our age model to reduce temporal uncertainty.

1004

1005 *Acknowledgements*

1006 We are grateful to the many people who helped make this study possible, Microtephra analysis was
1007 performed by Paola Del Carlo, Antonella Bertagnini, Alessio di Roberto of INGV, Pisa, Italy. Cores

1008 were processed at LACORE, Minneapolis with assistance from Anders Noren, Christina Brady, Amy
1009 Mybro and Jessica Heck. Figure 1 was created by Emanuele Ziaco. Funding was provided by the
1010 National Science Foundation (GSS-1228126) to Mensing and Noble, international travel awards and
1011 sabbatical leave from the University of Nevada, Reno to Mensing, the Sabina Universitas and
1012 Province of Rieti. We are grateful to Luigi Sandoletti for technical support, Giulia Sandoletti for
1013 laboratory assistance, Emanuele Presutti Saba, Emanuele Ziaco, and Gianluca Bonavigo for field and
1014 coring assistance, and DAFNE Università degli Studi della Tuscia for field transportation. Paolo
1015 Bellezza, Maurizio Sterpi at the Riserva Naturale dei Laghi Lungo e Ripasottile provided housing at
1016 the field site and boat access to Lago Lungo. Stefano Pizetti helped arrange housing in Viterbo for
1017 U.S. participants. Comments from an anonymous reviewer significantly improved the manuscript.

1018

1019 *Contributions by Authors*

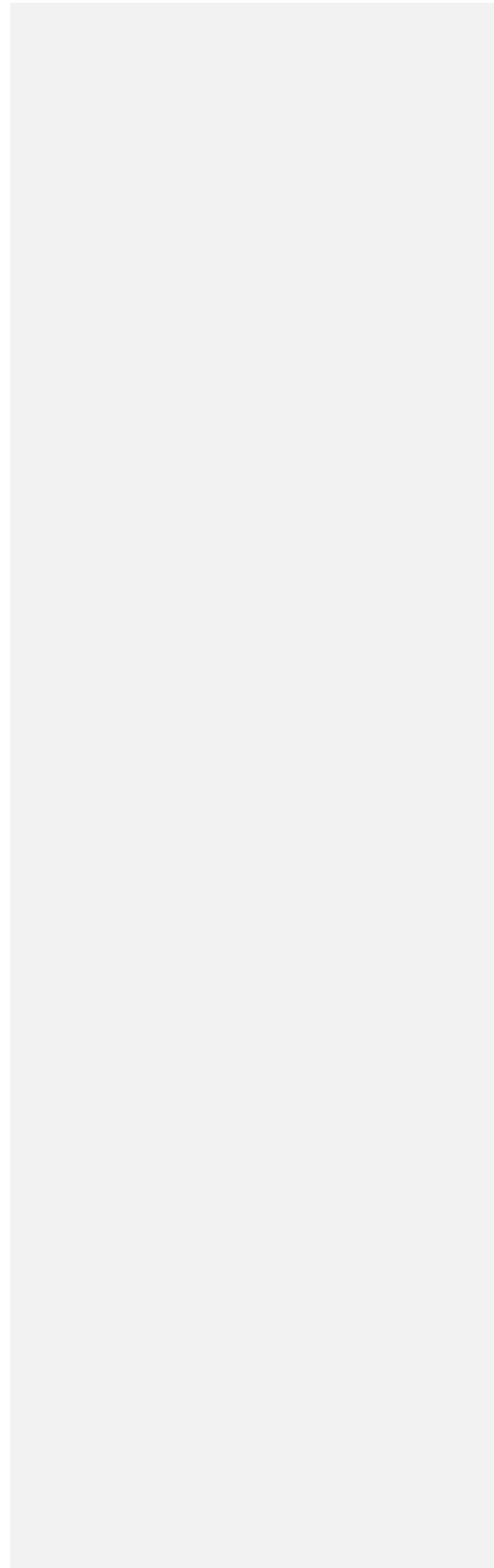
1020 Mensing co-led the field coring, analyzed pollen and contributed to development of the age model
1021 and climate proxy framework; Tunno assisted in field coring and analyzed pollen and charcoal;
1022 Sagnotti and Florindo conducted all rock magnetism and paleomagnetism analyses and developed
1023 the PSV age model; Noble created the core description, conducted smear slide analysis and analyzed
1024 elemental chemistry; Archer analyzed elemental chemistry; Zimmerman conducted all ^{14}C
1025 radiocarbon analyses and helped develop the age model; Pavón-Carrasco helped develop the age
1026 model and associated error analysis; Cifani and Passigli conducted historical archival research
1027 (Section 3.7) and contributed interpretation of historical documents, and specifically authored
1028 historical sections in part 5.2; Piovesan coordinated all Italian research components, co-led the field
1029 coring, interpreted pollen results in relation to local forest ecology, contributed to development of
1030 the age model and climate proxy framework and contributed to historical research. All co-authors
1031 contributed to writing the manuscript.

1032

1033

1034

41



1035 **References**

1036

1037 Aimers, J., 2011. Drought and the Maya; The story of artefacts. *Nature* 479, 4-5.

1038 Alfani, G., 2010. Pestilenze e 'crisi di sistema' in Italia tra XVI e XVII secolo. Perturbazioni di breve

1039 periodo o cause di declino economico?", in S. Cavaciocchi (ed.), *Le interazioni fra economia e*1040 *ambiente biologico nell'Europa preindustriale*, Florence University Press, Florence.1041 Alvino, G., Leggio, T., 2006. Acque e culti salutaris in Sabina, in *Usus veneratioque fontium 2006*

1042 Alvino, G., Leggio, T., 1997. Controllo idrogeologico e costruzione del paesaggio nella Sabina dalla

1043 prima età romana al medioevo, in *Uomo, acqua e paesaggio (Atti S. Maria Capua Vetere 1996)*,

1044 Roma, 89-98.

1045 Barbiera, I., Dalla-Zuanna, G., 2009. Population Dynamics in Italy in the Middle Ages: New Insights

1046 from Archaeological Findings, *Popul. and Dev. Rev.*, 35, 367-389.

1047 Berglund, B.E., 2003. Human impact and climate changes—synchronous events and a causal link?,

1048 *Quat. Int.*, 105, 7-12.

1049 Bersani, P., Bencivenga, M., 2001. Le piene del Tevere a Roma dal V secolo a.C. all'anno 2000, Roma:

1050 Presidenza del Consiglio dei Ministri: 8.

1051 Beug, H.J., 2004. Leitfaden der Pollenbestimmung für Mitteleuropa und angrenzende Geiete. Pfiel

1052 (ed.), München, 542.

1053 Blackmore, S., Steinmann, J.A.J., Hoen, P.P., Punt, W., 2003. The Northwest European Pollen Flora,

1054 65. Betulaceae and Corylaceae. *Rev. of Palaeob. and Palynol.*, 123, 71-98.

1055 Bottema, S. 1975. The interpretation of pollen spectra from prehistoric settlements (with special

1056 attention to Liguliflorae). *Palaeohistoria*, 57, 17-35.

1057 Branch, N. P., Marini, N. A., 2013. Mid-Late Holocene environmental change and human activities in

1058 the northern Apennines, Italy. *Quat. Int.*,

- 1059 Brown, A. G., Hatton, J., Selby, K. A., Leng, M. J., Christie, N., 2013. Multiproxy study of Holocene
1060 environmental change and human activity in the Central Apennine Mountains, Italy. *J Quat Sci*,
1061 28,1, 71-82.
- 1062 Bruce-Chwatt, L. J. and de Zulueta J. 1980. *The Rise and Fall of Malaria in Europe*. Oxford, Oxford
1063 University Press.
- 1064 Büntgen, U., Teleg, W., Nicolussi, K., McCormick, M., Frank, D., Trouet, V., Kaplan, J.O., Herzog, F.,
1065 Heussner, K.-U., Wanner, H., Luterbacher, J., Esper, J., 2011. 2500 years of European climate
1066 variability and human susceptibility. *Science*, 311, 578-582.
- 1067 Caciorgna, M.T. 1998. Popolamento e agricoltura: aspetti della politica territoriale del comune di
1068 Rieti nel Duecento. In M.G. Grillotti di Giacomo and L. Moretti (eds.), *I valori dell'agricoltura*
1069 *nel tempo e nello spazio*, vol. I, Brigati, pp. 82-97.
- 1070 Caciorgna, M.T. 2000. Confini e giurisdizioni tra Stato della Chiesa e Regno. In E. Hubert (ed.), *Une*
1071 *région frontalière au Moyen Âge. Les Vallées du Turano et du Salto entre Sabine et Abruzzes*,
1072 Paris, pp. 307-326.
- 1073 Calderini, G., Calderoni, G., Cavinato, G.P., Gliozzi, E., Paccara, P., 1998. The upper Quaternary
1074 sedimentary sequence at Rieti Basin (central Italy): a record of sedimentation response to
1075 climatic changes. *Palaeogeogr., Palaeoclimatol., Palaeoecol.*, 140, 97-111.
- 1076 Calderoni, G., Carrara, C., Ferrel, L., Follieri, M., Gliozzi, E., Magri, D., Narcisi, B., Parotto, M., Sadori,
1077 L., Serva, L., 1994. Palaeoenvironmental, palaeoclimatic and chronological interpretations of a
1078 late Quaternary sediment core from Piana di Rieti (central Apennines, Italy). *Giorn. Geol.*, 3,
1079 56/2, 43-72.
- 1080 Camerieri, T. M. 2011. Transumanza e agro centuriato in alta Sabina, interferenze e soluzioni
1081 gromatiche, in *Lazio e Sabina* 7, 111-127.
- 1082 Capasso, S., Malanima, P., 2007. Economy and population in Italy 1300-1913, *Popol. Stor.* 2, 15-40.
- 1083 Caprioli, M., 2008. *Lo statuto della città di Rieti: dal secolo XIV al secolo XVI*. Istituto storico italiano
1084 per il Medio Evo.

- 1085 Casella, L., Agrillo, E., Spada, F., 2009. Descrizione del patrimonio botanico e proposte di gestione
1086 della riserva naturale regionale Laghi Lungo e Ripasottile e della ZPS. La riserva naturale dei
1087 Laghi Lungo e Ripasottile, conoscenza e pianificazione, Rieti.
- 1088 Cavinato, G., De Celles, P. 1999. Extensional basins in the tectonically bimodal central Apennines
1089 fold-thrus belt, Italy: Response to corner flow above a subducting slab in retrograde motion.
1090 *Geology* 27, n. 10, 955-958.
- 1091 Celetti, D. 2007. La canapa nella Repubblica veneta. Produzione nazionale e importazione in età
1092 moderna. Istituto veneto di Scienze, Lettere ed Arti, Venezia.
- 1093 Chester, P.I., Raine, J.I., 2001. Pollen and spore keys for Quaternary deposits in the northern Pindos
1094 Mountains, Greece. *Grana*, 40:6, 299-387.
- 1095 Christiansen, B, Ljungqvist, F. 2012. The extra-tropical Northern Hemisphere temperature in the last
1096 two millenia: reconstructions of low-frequency variability. *Clim. Past* 8, 765-786.
- 1097 Cifani, G. 2003. Storia di una frontiera. Dinamiche territoriali e gruppi etnici nella media valle tiberina
1098 dalla prima età del ferro alla conquista romana. Roma: Istituto Poligrafico e Zecca dello Stato.
- 1099 Coccia, S., Mattingly, D.J., Beavitt, P., Elton, H., Foss, P. George, I., Hunt, C.O., Leggio, T., Patterson,
1100 H., Roberts, P., Brehm, T., Sudell, T., Sherratt, M. and Morton, K. 1992. Settlement History,
1101 Environment and Human Exploitation of an Intermontane Basin in the Central Apennines: The
1102 Rieti Survey 1988-1991, Part I. *Papers of the British School at Rome*, 60, 213-289.
- 1103 Coccia, S., Mattingly, D. J., Brehm, B., Elton, H., Foss, P., George, I., Leggio, T., Patterson, H., Roberts,
1104 P., Sudell, T., 1995. Settlement History, Environment and Human Exploitation of an
1105 Intermontane Basin in the Central Apennines: The Rieti Survey 1988-1991, Part II. Land-Use
1106 Patterns and Gazetteer. *Papers of the British School at Rome*, 63, 105-158.
- 1107 Coombes, P.M.V., Chiverrell, R.C. and Barber K. 2009. A high-resolution pollen and geochemical
1108 analysis of late Holocene human impact and vegetation history in southern Cumbria, England.
1109 *Journal of Quaternary Science*, 24(3), 224-236.

- 1110 Cosentino, D., Cipollari, P., Marsili, P. and Scrocca, D. 2010. Geology of the central Apennines: a
1111 regional review. In: (Eds.) Marco Beltrando, Angelo Peccerillo, Massimo Mattei, Sandro
1112 Conticelli, and Carlo Doglioni, *The Geology of Italy: tectonics and life along plate margins*,
1113 *Journal of the Virtual Explorer, Electronic Edition*, ISSN 1441-8142, volume 36, paper 12,
1114 doi:10.3809/jvirtex.2010.00223.
- 1115 Costambeys, M., 2009. Settlement, Taxation and the Condition of the Peasantry in Post-Roman
1116 Central Italy. *J. Agrar. Chang.*, 9(1), 92-119.
- 1117 Covino, R. 1995. L'invenzione di una regione. L'Umbria dall'Ottocento a oggi, p.142. Quattroemme
1118 Editore, Perugia.
- 1119 Croudace, I.W., Rindby, A., Rothwell, R.G., 2006. ITRAX; description and evaluation of a new multi-
1120 function X-ray core scanner. *Geol. Soc. Spec. Publ.*, 267, 51-63.
- 1121 Cugny, C., Mazier, F., Galop, D., 2010. Modern and fossil non-pollen palynomorphs from the Basque
1122 mountains (western Pyrenees, France): the use of coprophilous fungi to reconstruct pastoral
1123 activity. *Veg. Hist. Archaeobot.*, 19, 391-408.
- 1124 Cutini, M., Cancellieri, L., Cioffi, M. T. and Licursi, C. 2010. Phytosociology and phytogeography of
1125 fragmented *Alnus glutinosa* forests in a Tyrrhenian district (Central Italy). *ecologia*
1126 *mediterranea*, 36(2), 56.
- 1127 Davidson, W., 1993. Iron and manganese in lakes. *Earth Sci. Rev.*, 24, 119-163.
- 1128 Dean, W. E. Jr., 1974. Determination of carbonate and organic matter in calcareous sediments and
1129 sedimentary rocks by loss on ignition: Comparison with other methods. *J. Sed. Petrol.* 44:242–
1130 248.
- 1131 Dearing J.A., Jones R.T., Shen J., Yang X., Boyle J.F., Foster G.C., Crook D.S., Elvin M.J.D., 2008. Using
1132 multiple archives to understand past and present climate-human-environmental interaction:
1133 the lake Erhai catchment, Yunnan Province, China. *Journal of Paleolimnology*, 40: 3-31.
- 1134 De Santis, A., Coarelli, F., 2009 *Reate e l'Ager Reatinus: Vespasiano e la Sabina: dalle origini*
1135 *all'impero*. Quasar ed., Roma, 192.

- 1136 DeMeo, M., 2006. "Tecniche Costruttive Murrare Medievale". L'Erma, Roma, 326.
- 1137 Di Rita, F., Melis, R. T. 2013. The cultural landscape near the ancient city of Tharros (central West
1138 Sardinia): vegetation changes and human impact. *J. Archaeol. Sci.*, 40(12), 4271-4282.
- 1139 Di Rita, F., Celant, A., Magri, D., 2010. Holocene environmental instability in the wetland north of the
1140 Tiber delta (Rome, Italy): sea-lake-man interactions. *J. Paleolimn.*, 44(1), 51-67.
- 1141 Di Rita, F, Magri, D. 2009. Holocene drought, deforestation, and evergreen vegetation development
1142 in the central Mediterranean: A 5500 year record from Lago Alimini Piccolo, Apulia, southeast
1143 Italy. *Holocene*, 19, 295-306.
- 1144 Dupré, T. E. 1939. Il lago Velino. Saggio storico-geografico, Consorzio di bonifica della Piana reatina
1145 nel decennale della legge Mussolini, Rieti.
- 1146 Esper, J., Frank, D., Büntgen, U., Verstege, A., Luterbacher, J. and Xoplaki, E., 2007. Long-term
1147 drought severity variations in Morocco, *Geophys. Res. Lett.*, 34, L17702,
1148 doi:10.1029/2007GL030844.
- 1149 Faegri, K. and Iversen, J. 1985. Textbook of Pollen Analysis 4th edition. Hafner Press, New York.
- 1150 Ferreli, L., Brunamonte, F., Filippi, G., Margheriti, L., Michetti, A.M., 1992. Studi Geologici Camerti,
1151 volume speciale, 1992/1, 127-135.
- 1152 Ferreli, L., Parotto, M., Serva, L., 1990. Evoluzione del reticolo idrografico nella Piana di Rieti degli
1153 ultimi 4000 anno. *Mem. Soc. Geol. Italia*, 45, 90-910.
- 1154 Fraser, E.D.G., 2010. Can economic, land use and climatic stresses lead to famine, disease, warfare
1155 and death? Using Europe's calamitous 14th century as a parable for the modern age, *Ecol.
1156 Econ.*, doi:10.1016/j.ecolecon.2010.02.010.
- 1157 Gabbrielli, A., 2007. Le vicende storiche e demografiche italiane come causa dei cambiamenti del
1158 paesaggio forestale. *Annali Accademia Italiana di Scienze Forestali*, 133-166.
- 1159 Gallet, Y., Genevey, A., Le Go, M., 2002, Three millennia of directional variations of the Earth's
1160 magnetic field in western Europe as revealed by archaeological artefacts, *Phys. Earth Planet.
1161 Inter.*, 131, 81-89, doi:10.1016/S0031-9201(02)00030-4.

- 1162 Galli, A. 1840. Cenni economico-statistici sullo stato pontificio con appendice. Discorso sull'agro
1163 romano e sui mezzi di migliorarlo. Tipografia Camerale, Roma.
- 1164 Galli, P., Naso, J. 2009. Unmasking the 1349 earthquake course (southern Italy): paleoseismological
1165 and archaeoseismological indications for the hAqua Juliae fault. *J. of Struct. Geol.* 31, 128-
1166 149.
- 1167 Giaccio, B., Messina, P., Sposato, A., Volaggio, M., Zanchetta, G., Galadini, F., Gori, S., Santacroce, R.,
1168 2009. Tephra layers from Holocene lake sediment of the Sulmona Basin, central Italy:
1169 implications for volcanic activity in Peninsular Italy and tephrostratigraphy in the central
1170 Mediterranean area. *Quat. Sci. Rev.* 28, 2710-2733.
- 1171 Giraudi, C., 2005. Late-Holocene alluvial events in the Central Apennines, Italy. *The Holocene*, 15,5,
1172 768-773.
- 1173 Giraudi, C. The Holocene record of environmental changes in the 'Stagno di Maccarese' marsh (Tiber
1174 river delta, central Italy). *The Holocene*, 22 (12), 1461-1471.
- 1175 Giraudi, C., Magny, M., Zanchetta, G., Drysdale, R.N., 2011. The Holocene climatic evolution of
1176 Mediterranean Italy: A review of the continental geological data. *The Holocene*, 21,1, 105-115.
- 1177 Grove, A. T. and Rackham, O. 2001. *The Nature of Mediterranean Europe: An Ecological History*. Yale
1178 University Press, New Haven.
- 1179 Guiot, J., Corona, C., 2010. Growing season temperatures in Europe and climate forcings over the
1180 past 1400 years. *PloS one*,5(4), e9972.
- 1181 Haenssler, E., Nadeau, M., Vött, A., Unkel, I., 2013. Natural and human induced environmental
1182 changes preserved in a Holocene sediment sequence from the Etoliko Lagoon, Greece: New
1183 evidence from geochemical proxies. *Quat. Int.* , 308–309, 89-104.
- 1184 Harris, W. V., 2013. Defining and Detecting Mediterranean Deforestation, 800BCE to 700CE. In *The*
1185 *Ancient Mediterranean Environment between Science and History*, Harris Ed, Brill Collections:
1186 Classical Studies E-Books Online, Collection 2013, 173-194.

- 1187 Heiri, O., Lotter, A., Lemcke, G. 2001. Loss on ignition as a method for estimating organic and
1188 carbonate content in sediments: reproducibility and comparability of results. *J. of Paleolim.* 25,
1189 101-110.
- 1190 Hughes, J. D., 2011. Ancient deforestation revisited. *J. Hist.Biol.*,44(1), 43-57.
- 1191 Hurrell, J. W., 1995. Decadal trends in the North Atlantic Oscillation: regional temperatures and
1192 precipitation. *Science*, 269(5224), 676-679.
- 1193 Joannin, S., Brugiapaglia, E., Beaulieu, J. L. D., Bernardo, L., Magny, M., Peyron, O., Vanni re, B.,
1194 2012. Pollen-based reconstruction of Holocene vegetation and climate in Southern Italy: the
1195 case of Lago di Trifoglietti. *Clim. Past Discuss.*, 8(3), 2223-2279.
- 1196 Joannin, S., Magny, M., Peyron, O., Vanni re, B., Galop, D. 2014. Climate and land-use change during
1197 the late Holocene at Lake Ledro (southern Alps, Italy). *The Holocene* 24 (5), 591-602.
- 1198 Kaltenrieder, P., Procacci, G., Vanni re, B., Tinner, W., 2010. Vegetation and fire history of the
1199 Euganean Hills (Colli Euganei) as recorded by Lateglacial and Holocene sedimentary series
1200 from Lago della Costa (northeastern Italy).*The Holocene*, 20(5), 679-695.
- 1201 Kaplan, J.O., Krumhardt, K.M., Zimmermann, N., 2009. The prehistoric and preindustrial
1202 deforestation of Europe, *Quat. Sci. Rev.*, 28, 3016-3034.
- 1203 Keenan-Jones, D. 2013. Large-scale water management projects in Roman Central-Southern Italy. *In*
1204 "The Ancient Mediterranean Environment between Science and History", ed. W.V. Harris, Brill,
1205 Boston. Pp. 233-256.
- 1206 Kirschvink, J.L., 1980. The least-squares line and plane and the analysis of paleomagnetic data,
1207 *Geophys. J. R. Astron. Soc.*, 62, 699-718.
- 1208 K hler. E. , Lange, E. 1979. A contribution to distinguish cereal from wild grass pollen grains by LM
1209 and SEM. *Grana*, 18, 133-140.
- 1210 Korte, M., Constable, C., Donadini, F., Holme, R., 2011. Reconstructing the Holocene geomagnetic
1211 field. *Earth Planet. Sci. Lett.*, 312(3), 497-505.

- 1212 Kylander, M. E., Ampel, L., Wohlfarth, B., Veres, D., 2011. High-resolution X-ray fluorescence core
1213 scanning analysis of Les Echets (France) sedimentary sequence: new insights from chemical
1214 proxies. *J. Quat. Sci.*, 26(1), 109-117.
- 1215 Ladurie, E. LeRoy, 1971. "Times of Feast, Times of Famine: A History of Climate since the Year 1000.
1216 Translated by Barbara Bray. Doubleday and Company, Inc., New York. 426 pp.
- 1217 Leggio, T. 1986. Ermanno dei Reichenau, l'alluvione del 1053, i laghi reatini e Giulio Cesare. Il
1218 territorio 2: 275-277.
- 1219 Leggio, T. 1989a. Forme di insediamento in Sabina e nel Reatino nel medioevo. Alcune
1220 considerazioni. *Bullettino dell'Istituto Storico Italiano per il Medio Evo e Archivio Muratoriano*,
1221 95, 165- 201.
- 1222 Leggio, T. 1989b. Le fortificazione di Rieti dall' altomedioevo al Rinascimento (sec. VI-XVI). *Quaderni di*
1223 *storia urbana et territoriali* 4. pp. 18-27. Rieti.
- 1224 Leggio, T. 1994. Momenti della riforma cistercense nella Sabina e nel Reatino tra XII e XIII secolo.
1225 *Rivista Storica del Lazio*, 2, 17-61.
- 1226 Leggio, T. 1995a. Trasformazioni del paesaggio dei monti Sabini dall'età romana al medioevo. In T.
1227 Leggio, M. Marini (eds) "Il paesaggio della conca reatina. Problemi ed esperienze di una ricerca
1228 multidisciplinare", pp. 51-70. Rieti.
- 1229 Leggio, T. 1995b. L'olivo e la Sabina tra età romana e medioevo. In *L'olivo in Sabina e nel Lazio. Storia*
1230 *e prospettive di una presenza culturale*, Roma, pp. 13-77.
- 1231 Leggio, T. 1998. Un difficile rapporto tra uomo e ambiente: il paesaggio della conca reatina tra boschi
1232 ed acque. In M.G. Grillotti di Giacomo and L. Moretti (eds.), *I valori dell'agricoltura nel tempo e*
1233 *nello spazio*, vol. I, Brigati, pp. 99-115.
- 1234 Leggio, T. 2000. Il territorio della Provincia di Rieti tra la tarda antichità e lo scorcio del Medioevo.
1235 *Rivista storica del Lazio, Quaderno*. VIII, 3, 27-43.
- 1236 Leggio, T. 2007 . Pesca ed acque nel medioevo reatino. Rieti : *Riserva Naturale dei Laghi Lungo e*
1237 *Ripasottile*, 67

- 1238 Leggio, T. and Serva, L. 1991. La bonifica della Piana di Rieti dall'età romana al Medioevo: influenze
1239 sui mutamenti del paesaggio. *Notiziario dell'Enea*, 25-26, 61-70.
- 1240 Leggio, T., Michetti, A.M., Serva, L. , Vittorini, E., 1989. Processi naturali ed attività antropica a
1241 confronto nei tempi storici: metodologie adottate e ricerche programmate in un'area
1242 campione (Conca di Rieti). *Memorie della Società Geologica Italiana*, 42, 61-66.
- 1243 Leone, A., 2004 . *Ambiente e territorio agroforestale: linee guida per la pianificazione sostenibile e*
1244 *gli studi di impatto ambientale*. Ed. Franco Angeli, vol.95.
- 1245 Lo Cascio, E., Malanima, P., 2005. Cycles and stability. Italian population before the demographic
1246 transition (225 B.C.-A.D. 1900). *Rivista di Storia Economica*, n.s. XXI 3,5-40.
- 1247 Lorenzetti, R., 1989. *Studi e materiali per una Storia Sociale e Economica della Sabina*. Ricerca
1248 dell'Istituto Eugenio Cirese promossa dalla Regione Lazio Assessorato alla Cultura, Rieti.
- 1249 Lorenzetti, R., 1990. *Lacus Velinus. Per la salubrità dell'aere et per l'abundantia. La bonifica dell'agro*
1250 *reatino dall'antico Lacus Velinus alla riorganizzazione del territorio*, Milano.
- 1251 Lorenzetti, R. 1994. *La Sabina. Il territorio di carta*, Roma.
- 1252 Lorenzetti, R. 2009. *La terra e le acque. Trasformazioni e persistenze del paesaggio della Valle*
1253 *Reatina*, Rieti.
- 1254 Magri, D., 2007. Advances in Italian palynological studies: late Pleistocene and Holocene records, *J.*
1255 *Geol. Soc. Swed.*, 129:4, 337-344.
- 1256 McCormick, M., Buntgen, U., Cane, M., Cook, E., Harper, K., Huybers, P., Litt, T., Manning, S.,
1257 Mayewski, A., More, A., Nicolussi, K., Tegel, W. 2012. Climate change during and after the
1258 Roman Empire: Reconstructing the past from scientific and historical evidence. *J. Of*
1259 *Interdisciplinary History*, 43:2, 169-220.
- 1260 McNeil, J. R. 1992. *Mountains of the Mediterranean World: An Environmental History*. Cambridge
1261 University Press, Cambridge.

- 1262 Mercuri, A. M., Accorsi, C. A. and Mazzanti, M. B., 2002. The long history of *Cannabis* and its
1263 cultivation by the Romans in central Italy, shown by pollen records from Lago Albano and Lago
1264 di Nemi. *Veg. Hist. Archaeobot.*, 11(4), 263-276.
- 1265 Moriondo, M., Trombi, G., Ferrise, R., et al. (2013). Olive trees as bio-indicators of climate evolution
1266 in the Mediterranean Basin. *Global Ecology and Biogeography*, 22(7), 818-833.
- 1267 Munoz S., Gajewski K., Peros M.C., 2010. Synchronous environmental and cultural change in
1268 prehistory of the northeastern United States. *PNAS*, 107 (51): 22008-22013.
- 1269 Nalepka, D. and Walanus, A. (2003). Data processing in pollen analysis. *Acta Palaeobotanica* 43, 125-
1270 134.
- 1271 Nاسpi, N., 2010. Il capitolo della Cattedrale nella vita economica e sociale della *civitas* reatina. PhD
1272 thesis. Università degli Studi di Sassari.
- 1273 Newnham, R.M., Vanderfoes, M.J., Garnett, M.H., Lowe, D.J., Prior, C., Almond, P.C., 2007. Test of
1274 AMS 14C dating of pollen concentrates using tephrochronology. *J. Quat. Sci.*, 22(1), 37-51. DOI:
1275 10.1002/jqs.1016.
- 1276 Nigrisoli, G. 1857. *Rivista dei più importanti prodotti naturali e manifatturieri dello Stato Pontificio.*
1277 *Tipografia Governativa Taddei, Ferrara.*
- 1278 O'Sullivan, P., 2008. The 'collapse' of civilizations: what paleoenvironmental reconstruction cannot
1279 tell us, but anthropology can. *The Holocene*, 18(1), 45-55.
- 1280 Och, L. M., Müller, B., Voegelin, A., Ulrich, A., Gottlicher, J., Steiniger, R., Mangold, S., Vologina, E.G.,
1281 and Sturm, M. 2012. New insights into the formation and burial of Fe/Mn accumulations in
1282 Lake Baikal sediments. *Chem. Geol.* 330–331, 244–259.
- 1283 Olsen, J., Anderson, N., Knudsen, M. 2012. Variability of the North Atlantic Oscillation over the past
1284 5,200 years. *Nature Geoscience* 5, 808-812.
- 1285 Parotto, M., and A. Praturlon, 1975. Geological summary of Central Apennines, Structural Model of
1286 Italy, edited by L. Ogniben, M. Parotto, and A. Praturlon, *Quad. Ric. Sci.*, 90, 257-306.

- 1287 Pavón-Carrasco, F. J., Osete, M.L., Torta, J.M., Gaya-Piqué, L.R., 2009. A regional archeomagnetic
1288 model for Europe for the last 3000 years, SCHA.DIF.3K: applications to archeomagnetic dating,
1289 *Geochem. Geophys. Geosyst.*, 10, Q03013, doi:10.1029/2008GC002244.
- 1290 Piovesan, G., Schirone, B., 2000. Winter North Atlantic oscillation effects on the tree rings of the
1291 Italian beech (*Fagus sylvatica* L.). *Int. J. of Bio-Meteorol.*, 44(3), 121-127.
- 1292 Piovesan, G., Biondi, F., Di Filippo, A., Alessandrini, A., Maugeri, M., 2008. Drought-driven growth
1293 reduction in old beech (*Fagus sylvatica* L.) forests of the central Apennines, Italy. *Glob. Ch.*
1294 *Biol.*, 14(6), 1265-1281.
- 1295 Piovesan, G., Biondi, F., Bernabei, M., Di Filippo, A., Schirone, B., 2005. Spatial and altitudinal
1296 bioclimatic zones of the Italian peninsula identified from a beech (*Fagus sylvatica* L.) tree-ring
1297 network. *Acta Oecologica*, 27(3), 197-210.
- 1298 Punt W., Malotau, M., 1984. The Northwest European Pollen Flora, 31. Cannabaceae , Moraceae
1299 and Urticaceae; *Rev. Palaeobot. Palynol.*, 42, 23-44.
- 1300 Punt, W., Johanna, A.A.B., Hoen, P.P., 1991. The Northwest European Pollen Flora, 45 Oleaceae.
1301 *Rev. Palaeobot. Palynol.* 69, 23-47.
- 1302 Riccardi, R. 2006. Studi geografici sui laghi Lungo, Ripasottile e Ventina. Quaderni della Riserva
1303 Naturale dei laghi Lungo e Ripasottile 1, 47 p.
- 1304 Roberts, A. P., 2006, High-resolution magnetic analysis of sediment cores: Strengths, limitations and
1305 strategies for maximizing the value of long-core magnetic data. *Phys. Earth Planet. Int.*, 156,
1306 162–178.
- 1307 Roberts, N., Stevenson, A.D., Davis, B., Cheddadi, R., Brewer, S., Rosen, A., 2004. Holocene climate,
1308 environment and cultural change in the circum-Mediterranean region, in: Battarbee, R. W.,
1309 Gasse, F., Stickley, C. E. (Eds.), *Past Climate Variability through Europe and Africa*
1310 (Developments in Paleoenvironmental Research). Kluwer Academic Publishers, Dordrecht, pp.
1311 343-362.

- 1312 Russo Ermolli, E., di Pasquale, G., 2002. Vegetation dynamics of south-western Italy in the last 28 kyr
1313 inferred from pollen analysis of a Tyrrhenian Sea core. *Veg. Hist. Archaeobot.*, 11(3), 211-220.
- 1314 Russo Ermolli, E., Romano, P., Ruello, M. R. and Barone Lumaga, M. R., 2014. The natural and
1315 cultural landscape of Naples (southern Italy) during the Graeco-Roman and Late Antique
1316 periods. *J. Archaeol. Sci.*, 42, 399-411.
- 1317 Russo Ermolli, E., Di Donato, V., Martín-Fernández, J.A., Orain, R., Lebreton, V., Piovesan, G., in
1318 press. Vegetation patterns in the Southern Apennines (Italy) during MIS 13: deciphering pollen
1319 variability along a NW-SE transect. *Review of Palaeobotany and Palynology*.
- 1320 Sabbatani, S. 2005. Tentativi di lotta al paludismo e alla malaria nel Medio Evo. Ruolo dei Monaci
1321 Benedettini e Cistercensi nella nascita della Medicina Monastica e nelle bonifiche ambientali
1322 nel Medio Evo. *Le infezioni in medicina*, 3, 196-207.
- 1323 Sadori, L., 1994. Pollen analysis. In: Calderoni G, Carrara C, Fen-eli L, Follieri M, Gliozzi E, Magri D,
1324 Narcisi B, Parotto M, Sadori L, Serva L. (eds) *Palaeoenvironmental, palaeoclimatic and*
1325 *chronological interpretations of a late Quaternary sediment core from Piana di Rieti (central*
1326 *Apennines, Italy)*. *Giorn Geol*, 56(2), 51-54
- 1327 Sadori, L., Jahns, S., Peyron, O., 2011. Mid-Holocene vegetation history of the central
1328 Mediterranean. *The Holocene*, 21 (1), 117-129.
- 1329 Sadori, L., Ortu, E., Peyron, O., Zanchetta, G., Vannière, B., Desmet, M., Magny, M., 2013. The last 7
1330 millennia of vegetation and climate changes at Lago di Pergusa (central Sicily, Italy). *Climate of*
1331 *the Past*, 9(4), 1969-1984.
- 1332 Sagnotti, L., 2013. Demagnetization Analysis in Excel (DAIE) - An open source workbook in Excel for
1333 viewing and analyzing demagnetization data from paleomagnetic discrete samples and u-
1334 channels. *Anna. Geophys.*, 56, 1, 2013, D0114; doi:10.4401/ag-6282.
- 1335 Sagnottis, L., Rochette, P., Jackson, M., Vadeboin, F., Dinarès-Turell, J., Winkler, A. 2003. Inter-
1336 laboratory calibration of low-field magnetic and anhysteretic susceptibility measurements.
1337 *Physics of the Earth and Planetary Interiors*, 138, DOI [10.1016/S0031-9201\(03\)00063-3](https://doi.org/10.1016/S0031-9201(03)00063-3).

- 1338 Sereni, E., 1973. Agricoltura e mondo rurale, in Storia d'Italia, I, I caratteri originali, Torino Einaudi
1339 (ed.), pp. 133- 252.
- 1340 Sisani, S. 2009 (ed). Nursia e l'ager Nursinus. Un distretto sabino dalla *praefectura* al *municipium*
1341 (catalogue of the exhibition, Norcia 2009), Roma: Quasar.
- 1342 Sköld, E., Lagerås, P. and Berglund, B.E. 2010. Temporal cultural landscape dynamics in a marginal
1343 upland area: agricultural expansions and contractions inferred from palynological evidence at
1344 Yttra Berg, southern Sweden. *Vegetation History and Archaeobotany*, 19, 121-136.
- 1345 Soligo, M., Tuccimei, P., Barberi, R., Delitala, M.C., Miccadei, E. and Taddeucci, A., 2002. U/Th dating
1346 of freshwater travertine from Middle Velino Valley (Central Italy): paleoclimatic and geological
1347 implications. *Palaeogeogr., Palaeoclimatol., Paleoecol.*, 184, 147-161.
- 1348 Spadoni, M., Brilli, M., Giustini, F., Petitta, M. 2010. Using GIS for modelling the impact of current
1349 climate trend on the recharge area of the S. Susanna spring (sentral Apennines, Italy). *Hydrol.*
1350 *Process.* 24, 50-64.
- 1351 Stockmarr, J., 1971. Tablets with spores used in absolute pollen analysis. *Pollen et Spores*, 13, 615-
1352 621.
- 1353 Sulpizio, R., Zanchetta, G., Caron, B., Dellino, P., Mele, D., Giaccio, B., Insinga, D., Paterne, M., Siani,
1354 G., Costa, A., Macedonio, G., Santacroce, R. 2014. Volcanic ash hazard in the central
1355 Mediterranean assessed from geological data. *Bull Volcanol* 76, 866- 874.
- 1356 Tennant, R.K., Jones, R.T., Brock, F., Cook, C., Turney, C.M., Love, J., Lee, R., 2013. A new flow
1357 cytometry method enabling rapid purification of fossil pollen from terrestrial sediments for
1358 AMS radiocarbon dating. *J. Quat. Sci.*, DOI: 10.1002/jqs.2606.
- 1359 Tinner, W., van Leeuwen, J., Colombaroli, D., Vescovi, E., van der Knaap, W., Henne, P., Pasta, S.,
1360 D'Angelo, S., Mantia, T. 2009. Holocene environmental and climatic changes at Gorgo Basso, a
1361 coastal lake in southern Sicily, Italy. *Quat. Sci. Rev.*, 28, 1498-1510.

- 1362 Torres, N.T., Och, L.M., Hauser, P.C., Furrer, G., Brandl, H., Vologina, E., Sturm, M., Bürgmann,
1363 Müller, B., 2014. Early diagenetic processes generate iron and manganese oxide layers in the
1364 sediments of Lake Bakail, Siberia. *Env. Science: Processes and Impacts*, 16 (4), 615-944.
- 1365 Tozzi, I., 2009. I riti funebri ed il pietoso ufficio della sepoltura a Rieti durante l'età moderna. *Storia*
1366 *del mondo*, 59.
- 1367 Trachsel, M., Kamenik, C., Grosjean, M., McCarroll, D., Moberg, A., Brázdil, R., Riemann, D. (2012).
1368 Multi-archive summer temperature reconstruction for the European Alps, AD 1053–
1369 1996. *Quaternary Science Reviews*, 46, 66-79.
- 1370 Trouet, V., Esper, J., Graham, N.E., Baker, A., Scourse, J.D., Frank, D.C., 2009. Persistent Positive
1371 North Atlantic Oscillation Mode Dominated the Medieval Climate Anomaly. *Science*, 324, 78.
- 1372 Van Benthem, F., Clarke, G.C.S., Punt, W., 1984. The Northwest European Pollen Flora, 33. Fagaceae.
1373 *Rev. Palaeobot. Palynol.*, 42, 87-110.
- 1374 van Geel, B., Aptroot, A. 2006. Fossil ascomycetes in Quaternary deposits. *Nova Hedwigia*, 82, 313-
1375 329.
- 1376 van Geel, B., Gelorini, V., Lyaruu, A., Aptroot, A., Rucina, S., Marchant, R., Sinninghe Damsté, J. S.,
1377 Verschuren, D., 2011. Diversity and ecology of tropical African fungal spores from a 25,000-
1378 year palaeoenvironmental record in southeastern Kenya. *Rev. Palaeobot. Palynol.*, 164, 174-
1379 190.
- 1380 van Hoof, T.B., Bunnik, F.P.M., Waucomont, J.G.M., Kürschner, W.M., Visscher, H., 2006. Forest re-
1381 growth on medieval farmland after the Black Death pandemic —Implications for atmospheric
1382 CO2 levels. *Palaeogeogr., Palaeoclimatol., Palaeoecol.*, 237, 396-411.
- 1383 Vecchio, B., 1974. *Il bosco negli scrittori italiani del Settecento e dell'età napoleonica*. Einaudi (ed.),
1384 Torino.
- 1385 Yeloff, D., van Geel, B., 2007. Abandonment of farmland and vegetation succession following the
1386 Eurasian plague pandemic of AD 1347-52. *J. Biogeogr.* 34, 575-582.

- 1387 Zuccagni-Orlandini, A. 1843. Corografia fisica, storica e statistica dell'Italia e delle sue isole :
- 1388 corredata di un Atalante di mappe geografiche e topografiche, e di altre tavole illustrative 10,[2]
- 1389 Supplemento. Editori, Firenze.
- 1390

1391

1392

1393 Fig. 1. Rieti Basin study site map.

1394

1395 Fig. 2. Correlation of cores 2A, 2B, and 2C based distinctive sedimentologic features.

1396 Livingston core sections are denoted for cores 2A and 2B. Shaded areas denote

1397 sections used in composite core, pictured in figure 3. 1 = oxidized band; 2 = discontinuously

1398 laminated dark silty marl; 3 = varicolored banded clay, silt, and carbonate; 4 = gray clay;

1399 5 = organic-rich marl with calcite stringers.

1400

1401 Fig. 3. High resolution images of the Lago Lungo Master core (LUN 12-2). Individual cores sections

1402 used in the master are labelled. White boxes represent core sections with no recovery. Running

1403 depth is a continuous measure (m) of the total core length.

1404

1405 Fig.4. ^{14}C AMS radiocarbon dates plotted in relation to the PSV age model used in this study. Colored

1406 bands are: green – Archaic to early Medieval; orange – Medieval; blue – LIA. Age model

1407 reconstructed by integrating constraints from pollen analysis, PSV and RPI curves (Table 1).

1408 Uncertainties represent the 65% and 95% of confidence levels according to the SCHA.DIF.3k model

1409 predictions (Pavón-Carrasco et al, 2009; Table 1). The analyzed sequence spans the last 2700 years

1410 with an average sedimentation rate of 5.8 mm yr^{-1} .

1411

1412 Fig. 5 Stratigraphic trends of k , NRM and ARM of the various cores, correlated to a common depth.

1413

1414 Fig. 6. Representative demagnetization diagrams. For the vector component diagrams, black (white)

1415 circles indicate projection on the horizontal (vertical) plane. When demagnetization steps are

1416 selected for PCA, the corresponding symbols turn to red (for horizontal projection) and to light blue

1417 (for vertical projections). The stereoplots are equal-area projections, with solid symbols representing
1418 points on the lower hemisphere. The plots showing the decay of the NRM intensity as a function of
1419 the demagnetization steps are shown on the right side of each equal-area projection. The cores were
1420 not azimuthally oriented and declinations are reported in the laboratory coordinate system with
1421 respect to the split face of the drill core.

1422

1423 Fig. 7. PSV trends for the measured cores, plotted as a function of the common depth and age. Age
1424 was estimated by correlation with PSV reference curves and models (Archeomagnetic data from
1425 France, Gallet et al. 2002; scha.dif.3k of Pavón-Carrasco et al. 2009). Prominent PSV features
1426 (inclination, declination and RPI shown in bold in Table 1) used for depth vs age correlation and
1427 cultigens (significant changes in forest phase, and appearance of *Zea mays* and *Cannabis* type) from
1428 the pollen data are marked by arrows.

1429

1430 Fig. 8. PSV trends for core LUN-12-1A and 1B, plotted as a function of the ^{210}Pb and ^{14}C AMS dates. In
1431 relation to the PSV reference curves and models (Archeomagnetic data from France, Gallet et al.
1432 2002; scha.dif.3k of Pavón-Carrasco et al. 2009).

1433

1434 Fig. 9. Principal components analysis biplots for core 12LUN-2 showing variations in elemental
1435 composition from XRF data: a) Medieval interval and b) Little Ice Age interval. Samples are plotted
1436 as open circles and eigenvectors for elements in red. Axis 1 is largely related to carbonate (- values)
1437 versus siliciclastic (+ values) component. 1) carbonate rich eigenvectors; 2) siliciclastic-rich
1438 eigenvectors; 3) redox eigenvectors.

1439

1440 Fig. 10. Geochemical and sedimentological parameters, including Loss on Ignition data (LOI),
1441 magnetic susceptibility, selected elemental data from XRF (reported in kilacounts per second).
1442 Sediment accumulation rate was calculated from the age model. Stratigraphic intervals discussed in

1443 text are abbreviated on the left; Modern Interval (MI), Little Ice Age (LIA), Medieval Period (MP),
1444 Transitional Zone (TR) between MP and RE, and Roman Era and Migration Period (RE). Boundaries of
1445 pollen zones (dashed lines) listed on right are also discussed in the text.

1446

1447 Fig. 11. Selected pollen taxa of trees, vines and shrubs, and total pollen accumulation rate. Unfilled
1448 lines represent 5X exaggeration.

1449 Fig. 12. Selected pollen taxa of herbs, crop plants and indeterminate pollen. Unfilled lines represent
1450 5X exaggeration.

1451

1452 Fig. 13. Selected aquatic pollen, algae, non-pollen palynomorphs and charcoal. Unfilled lines
1453 represent 5X exaggeration.

1454

1455 Fig. 14. Summary diagram with selected data. Arboreal pollen includes all tree taxa presented in Fig.
1456 11 except *Alnus*. Disturbance taxa include all herbs plus trilete ferns shown in Fig. 12. Diatoms were
1457 identified from smear slide analysis. Stratigraphic intervals follow Fig. 10. Büntgen et al . (2011)
1458 climate proxy series were smoothed with a lowpass filter that blocked frequencies > 0.016 (Hammer,
1459 \emptyset ., Harper, D.A.T., Ryan, P.D. 2001. PAST: Paleontological statistics software package for education
1460 and data analysis. *Palaeontologia Electronica* 4(1): 9pp. [http://palaeo-](http://palaeo-electronica.org/2001_1/past/issue1_01.htm)
1461 [electronica.org/2001_1/past/issue1_01.htm](http://palaeo-electronica.org/2001_1/past/issue1_01.htm)).

1462